ELSEVIER

Contents lists available at ScienceDirect

Journal of Hydrology

journal homepage: www.elsevier.com/locate/jhydrol



Research papers

Groundwater geochemistry and flow in the Spring Mountains, NV: Implications for the Death Valley Regional Flow System



Sara R. Warix^a, Laura K. Rademacher^a, Zachary P. Meyers^b, Marty D. Frisbee^b

- ^a Department of Geological and Environmental Sciences, University of the Pacific, 3601 Pacific Avenue, Stockton, CA 95211, United States
- b Department of Earth, Atmospheric, and Planetary Sciences, Purdue University, 550 Stadium Mall Drive, West Lafayette, IN 47907, United States

ARTICLE INFO

This manuscript was handled by Huaming Guo, Editor-in-Chief, with the assistance of Seong-Taek Yun, Associate Editor

Keywords: 87 Sr/86 Sr Geochemical weathering Interbasin groundwater flow Spring Mountains Death Valley Regional Flow System

ABSTRACT

Groundwater geochemistry and 87Sr/86Sr from spring waters in the Spring Mountains, NV were used to understand how groundwater recharging in the Spring Mountains influences regional groundwater flow in the Death Valley Regional Flow System (DVRFS). Previous researchers hypothesized that groundwater from the Spring Mountains contributes to the DVRFS, an interbasin groundwater flow system (IGF). However, the Spring Mountains are geologically heterogeneous, therefore, a uniform contribution of groundwater flow across the range is unlikely. Here, we use spring water geochemistry, spring water and host rock 87Sr/86Sr, and observations of the surrounding geology to determine what regions of the Spring Mountains are likely to contribute more flow to the DVRFS. Based on geochemical and isotopic evidence, Spring Mountains groundwater can be divided into three flow regions with distinct geochemical signals reflecting silicate or carbonate water-rock interactions and location relative to major thrust faults. The Keystone Thrust flow region (KST) has a 87Sr/86Sr of 0.710-0.711, is recharged by both rain and snow, and weathers both Mesozoic sandstones and Permian and Cambrian carbonate. Central Spring Mountains (CSM) groundwater has a $^{87}\text{Sr}/^{86}\text{Sr}$ of ~ 0.708 , is primarily recharged by snow, and weathers Permian and Cambrian limestones and dolostones. The Montgomery Hills (MH) flow region has a 87 Sr/ 86 Sr 0.711–0.733, is recharged by both rain and snow, and weathers both Permian and Cambrian carbonates and Precambrian siliciclastics. Groundwater mixing between flow groups occurs along major thrust faults in the study area, as evidenced by 87 Sr/ 86 Sr signatures that reflect one flow group and δ^{18} O and δ^2H and geochemical signatures that reflect another flow group. The combination of geochemical and isotopic results suggest CSM groundwater is the most likely to reach Death Valley because CSM groundwater composition reflects the geochemical and isotopic signatures of the highly permeable rocks that connect the Spring Mountains to Death Valley. Flow leaving the KST and MH also influences the DVRFS after mixing with CSM groundwater along major thrust faults.

1. Introduction

The concept of interbasin groundwater flow (IGF) is well established (Frisbee et al., 2016; Genereux et al., 2013, 2002; Pacheco, 2015; Stewart-Maddox et al., 2018; Tóth, 1999, 1995, 1963). IGF occurs when groundwater flow crosses surface water drainage divides and discharges in an adjacent topographic basin. Although sedimentary bedrock may be naturally conducive to the occurrence of IGF (Frisbee et al., 2016; Stewart-Maddox et al., 2018), it can occur in different geologic

settings. For example, IGF was observed in watersheds underlain by volcanic bedrock in Costa Rica (Genereux et al., 2013, 2002), in volcanic, volcaniclastic, and sedimentary rocks of the lower Rio Grande Valley in New Mexico (Langman and Ellis, 2010), and in Quaternary sediments in Denmark (Danapour et al., 2019). Local- and intermediate-scale flowpaths are interpreted to contribute to regional groundwater flow systems through large faults and contact zones (Pacheco and Van der Weijden, 2014a). Recent studies identify IGF as an integral component of the Death Valley Regional Flow System (DVRFS) in the

Abbreviations: CSM, Central Spring Mountains; KST, Keystone Thrust; LCA, Lower carbonate-rock aquifer; SCU, Sedimentary rock confining unit; LCCU, Lower clastic-rock confining unit; DVRFS, Death Valley Regional Flow System; IES, Integrated Earth Systems (spring naming convention); IGF, Interbasin Groundwater Flow; MH, Montgomery Hills

^{*}Corresponding author at: Department of Geosciences, Idaho State University, 921 S. 8th Ave, Pocatello, ID 83201, United States. E-mail address: warisara@isu.edu (S.R. Warix).

S.R. Warix, et al. Journal of Hydrology 580 (2020) 124313

deserts of southern Nevada and eastern California (Anderson et al., 2006; Belcher and Sweetkind, 2010; Nelson et al., 2004; Nelson and Mayo, 2014; Stetzenbach et al., 1999; Thomas et al., 2013).

The DVRFS is an extensive and complex regional set of aquifers in southern Nevada and southeastern California (Belcher and Sweetkind, 2010). Groundwater in the DVRFS is recharged at high elevations in the Spring Mountains and other central and southern Nevada uplands (Pahranagat Range, Sheep Range, Quinn Canyon Range, etc.) and supplies flow to high discharge springs in desert basins such as Death Valley and Amargosa Valley (Belcher et al., 2009; Bushman et al., 2010; Thomas et al., 2013). Understanding the magnitude and geographic extent of IGF connectivity and spring permanence is important for groundwater management and planning (Belcher et al., 2009), particularly in the arid southwest where high temperatures and low annual recharge limit the presence of surface water. Additionally, climate change is altering recharge patterns in arid regions (Akiyama et al., 2018; Love and Zdon, 2018; McKenna and Sala 2018). Recharge to the DVRFS is expected to decrease (Meixner et al., 2016), yet desert communities and groundwater-dependent ecosystems rely on groundwater as the primary, sometimes only, source of perennial freshwater (Klausmeyer et al., 2018; Patten et al., 2008). Despite the importance of groundwater in the region, the contributing areas to and groundwater fluxes in the DVRFS are still debated (Anderson et al., 2006; Belcher et al., 2009; Belcher and Sweetkind, 2010; Burbey, 1997; Bushman et al., 2010; D'Agnese et al., 1998; Hevesi et al., 2003).

Research in the DVRFS region has utilized water chemistry, isotopes, and various modeling techniques to quantify and delineate groundwater flowpaths that contribute to basin springs as part of the large IGF network (Belcher and Sweetkind, 2010; Bushman et al., 2010; Peterman et al., 1992; Thomas et al., 2013; Ye et al., 2016). The Spring Mountains are the highest range in the DVRFS and receive a relatively large annual precipitation from both winter snow and summer rainfall (Winograd et al., 1998). The Spring Mountains receive substantial modern recharge that supplements the paleorecharge in storage (Hershey et al., 2016) and provides hydraulic forcing necessary for sustaining flow in the DVRFS. Indeed, previous studies indicate that the Spring Mountains, NV are one of the greatest sources of recharge in the DVRFS (Belcher et al., 2009; Belcher and Sweetkind, 2010; Bushman et al., 2010; Hevesi et al., 2003; Larsen et al., 2001; Stetzenbach et al., 1999; Thomas et al., 2013; Tiedeman et al., 2003; Winograd et al., 1998; Winograd and Pearson, 1976). While regional research is abundant, detailed hydrogeologic studies focused on the geochemistry of Spring Mountains groundwater as it relates to the DVRFS are scarce and often lack incorporation of structural controls and applications of environmental tracers, which can be used to infer connectivity of flowpaths (Hershey, 1989; Hershey et al., 2016; Hughes, 1966).

In this study, Spring Mountains groundwater was evaluated as a contributing influence to the DVRFS by use of water stable isotopes ($\delta^{18}O$ and $\delta^{2}H$), general geochemistry, and $^{87}Sr/^{86}Sr$ of spring water and rock units thought to host flowpaths measured at twelve springs, along with observations from published geologic maps and cross sections. Specifically, this project aims to: (1) identify recharge areas and potential mixing between groundwater regions; (2) characterize the geochemistry of Spring Mountains springs; (3) understand the influence of geology on groundwater flow; and (4) identify the region of Spring Mountains most likely to contribute groundwater to the DVRFS.

2. Study area

The Spring Mountains are a northwest-southeast trending mountain belt in southwestern Nevada between the cities of Las Vegas, NV and Pahrump, NV (Fig. 1). The mountain belt lies in the southern Great Basin physiographic province and spans more than $80\,\mathrm{km}$ in length with over $2200\,\mathrm{km}^2$ of mountainous terrain. The Spring Mountains are the highest mountain range in southern Nevada (Mt. Charleston = $3632\,\mathrm{masl}$) and exhibit significant relief from adjacent basins

(Pahrump ≈ 800 masl, Las Vegas ≈ 600 masl).

2.1. Climate and precipitation

The large relief of the Spring Mountains causes climate patterns to vary with elevation; alluvial valleys are arid lowland deserts while high elevations have a climate similar to an alpine tundra (Hershey, 1989). The Spring Mountains receive significant recharge despite their location in the rain shadow of the Sierra Nevada (Hevesi et al., 2003). Average annual precipitation ranges from 20 cm in the foothills up to greater than 70 cm at mountain crests (Moreo et al., 2014; Winograd et al., 1998; Winograd and Thordarson, 1975). Winograd et al. (1998) classify precipitation events into two types, 1) low-pressure winter storms that originate over the Pacific Ocean and 2) short and intense summer storms that originate from the Gulf of California and the Gulf of Mexico. Stable isotope evidence from prior studies (Springer et al., 2016; Winograd et al., 1998) suggests that both summer and winter storms contribute to groundwater flow; however, late spring snowmelt constitutes the greatest proportion (>90 percent) of recharge. Mean annual air temperatures are also variable, particularly across the elevation gradient of the Spring Mountains. The average annual temperature at Lee Canyon from 2009 to 2017 (2414 m) was 9.5 °C (NOAA-NCDC, 2019). In the adjacent southwest basin, the average annual temperature of Pahrump is 17.3 °C with summer highs approaching 40 °C (NOAA-NCDC, 2019). Consequently, vegetation also varies with elevation (Moreo et al., 2014). At low elevations desert shrubs dominate the environment. As elevation increases, vegetation transitions to a juniperpinyon woodland environment and eventually to a coniferous forest and alpine tundra (Hershey, 1989).

Spring Mountains groundwater is an important water resource for local communities and ecosystems and provides freshwater to the nearby cities of Las Vegas, NV (Las Vegas Valley Water District, 2018) and Pahrump, NV (Harrill, 1986; Nye County Water District, 2018). Rainfall and surface water are limited in the southern Great Basin; therefore, desert ecosystems are dependent on a stable discharge of groundwater as a reliable source of freshwater. Indeed, Spring Mountains springs host highly productive groundwater-dependent ecosystems (Kreamer et al., 2015). In addition to recharging the underlying aquifer and supplying local springs with groundwater flow, the Spring Mountains conduct mountain front recharge to the basinal aquifer systems to the east and southwest (Harrill, 1986; Morgan and Dettinger, 1994).

2.2. Geology

The Spring Mountains comprise a sequence of sedimentary strata deposited upon the Paleozoic passive margin of western North America. These strata have since been displaced by thrust and normal faults, uplifted, and deeply eroded, exposing the regional carbonate aquifer that underlies much of the southern Great Basin (Figs. 1 and 2). From northwest to southeast, strata transition up-section from Precambrian siliciclastic rocks to Paleozoic dolostone and limestone to Mesozoic sandstones. The Sevier orogeny generated folds and northeast-southwest trending thrust faults, namely the Keystone Thrust, Lee Canyon Thrust, and the Wheeler Pass Thrust (Burchfiel et al., 1974). Basin and Range extension caused northwest-southeast trending normal faults to cut existing thrust faults (Page et al., 2005).

Four major rock types dominate the Spring Mountains: sandstone, limestone, dolostone, and siliciclastic rocks (Table 3). Mesozoic sandstones are present in the eastern Spring Mountains near the Keystone Thrust (KST) and are the youngest rocks in the mountain belt. In addition to sandstone, evaporite lenses found in Mesozoic units are observed to influence groundwater geochemistry where present (Hershey, 1989). Limestone and dolostone are abundant at the highest elevations in the central Spring Mountains (CSM). Typically, limestone units are younger than down-section dolostone units. The Bird Spring Formation

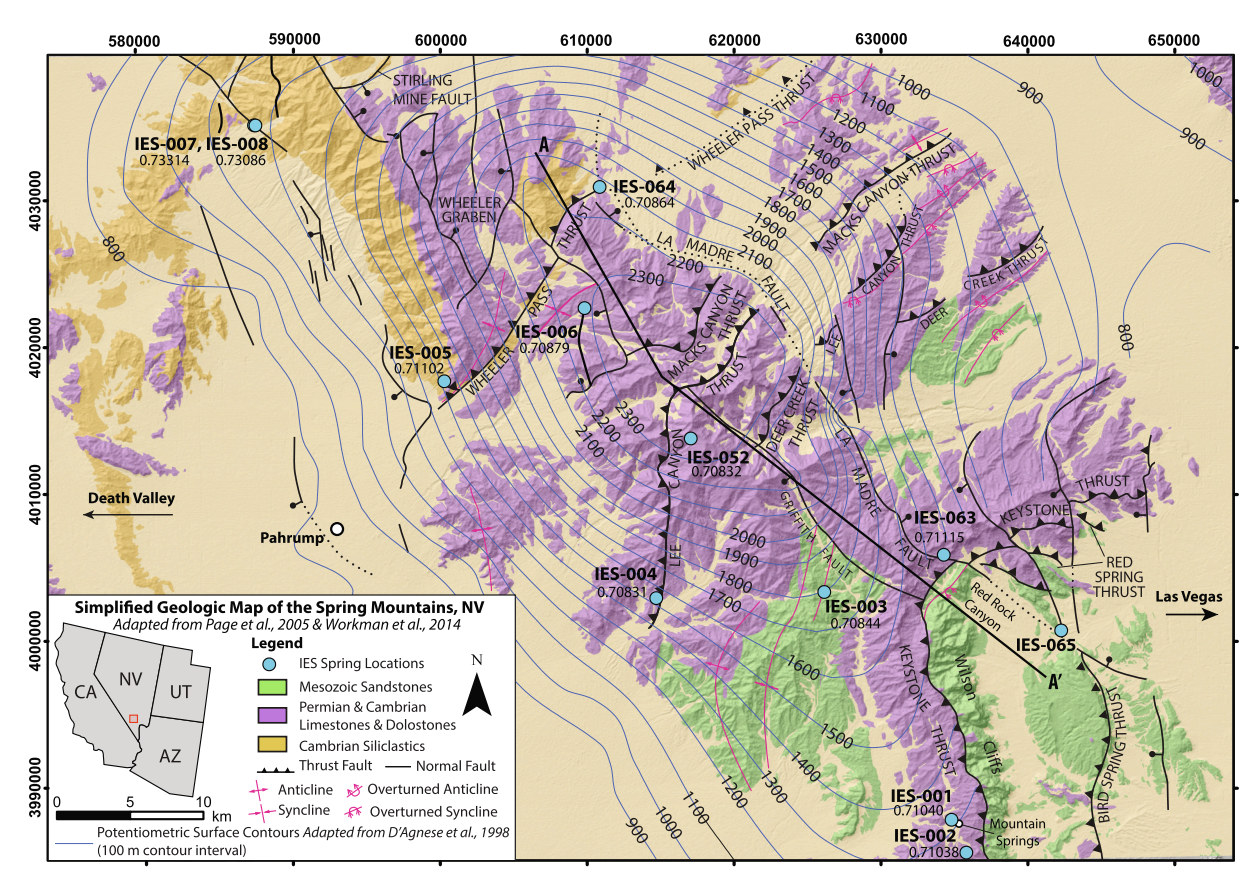


Fig. 1. Simplified geologic map of the Spring Mountains adapted from Page et al. (2005) and Workman et al. (2016) Rocks units are colored by their primary composition and age; color breakdown is listed in Table 3. Green units are Mesozoic sandstones, purple units are Permian and Cambrian dolostone and limestone, yellow units are Cambrian and Precambrian siliciclastics. Springs are plotted as blue dots with their corresponding sample names (IES-XXX) and the relevant ⁸⁷Sr/⁸⁶Sr listed below each spring point. Major structural features are displayed as identified and adapted from Geologic and Geophysical maps of the Las Vegas 30′x 60′ Quadrangle, Clark and Nye Counties, Nevada, and Inyo County, California (Page et al., 2005) and (Workman et al., 2016). Potentiometric contours adapted from (D'Agnese et al., 1998) are displayed in dark blue. The cross-section A-A' is displayed in Fig. 2. (For interpretation of the references to color in this figure legend, the reader is referred to the web version of this article.)

is commonly surficially exposed in the CSM and has a maximum exposed thickness of 2355 m suggesting its importance for recharging groundwater (Page et al., 2005). The northwest Spring Mountains, referred to as the Montgomery Hills (MH), comprise the oldest rocks in

the mountain belt and are located northwest of the Wheeler Pass Thrust. The Montgomery Hills are predominately quartzite, but also include siltstone, sandstone, shale, and minor dolostone and limestone beds. Rocks in the Montgomery Hills are commonly brecciated.

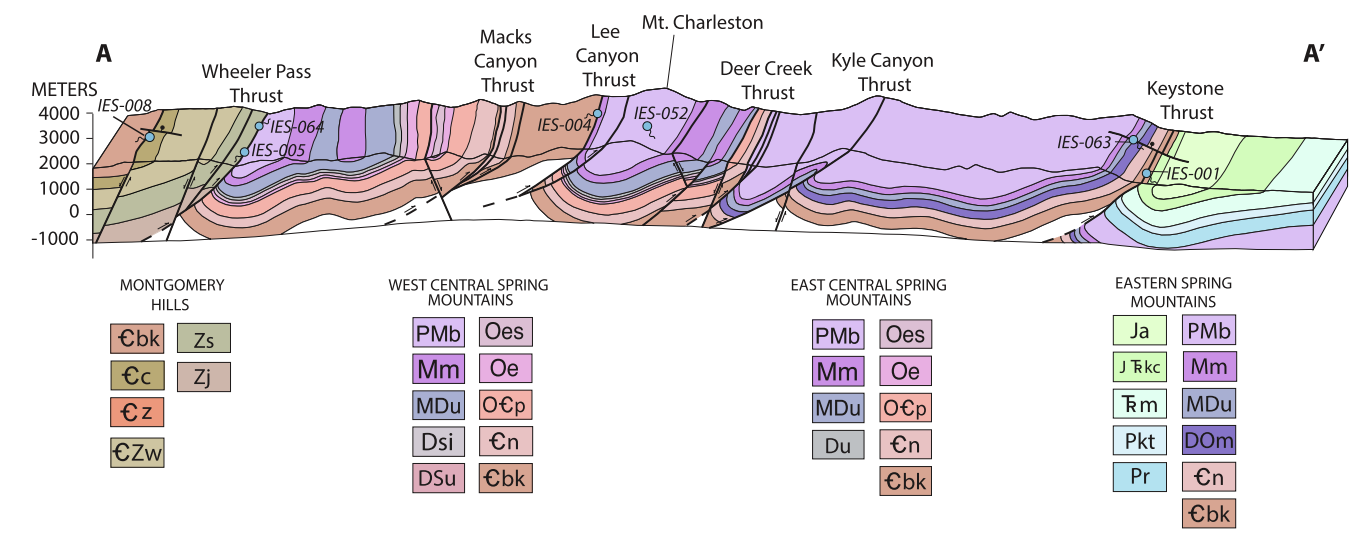


Fig. 2. Block diagram cross section from A to A' (Fig. 1) adapted from Page et al. (2005). Springs emergence locations are approximate. Geologic units for four regions in the Spring Mountains are listed below the block diagram for the portion of the Spring Mountains they represent. Geologic unit abbreviations are defined in Table 3.

Journal of Hydrology 580 (2020) 124313

Table 1
List of sampled springs and field and lab metrics. Temperature was recorded in field with a YSI Pro Plus. Specific conductance and pH were determined in lab by the New Mexico Bureau of Geology & Mineral Resources Analytical Chemistry Laboratory. Flow region abbreviations are as follows: Keystone Thrust = KST, Central Spring Mountains = CSM, Montgomery Hills = MH. *Temperature was not collected at the spring and was instead supplemented with data from the USGS (USGS 361541115415001 and USGS 360840115251001) (USGS, 2019).

IES Number	Spring Name	Sample Date	Easting	Northing	Elevation (m)	Temperature (°C)	pН	Specific Conductance (µS/cm)	Flow Region
IES-001	Mountain Spring	3/12/16	634808	3987716	1688	17.2	8.1	911	KST
IES-002	Potosi/BSA Spring	3/12/16	635816	3985472	1648	9.9	7.9	593	KST
IES-003	Cave Spring	3/13/16	626122	4003263	1950	9.5	7.5	670	CSM
IES-004	Kiup Spring	3/13/16	614662	4002847	1571	15.9	7.4	756	CSM
IES-005	Horse Spring	3/13/16	600198	4017646	1518	16.9	7.7	539	MH
IES-006	Buck Spring	3/14/16	609764	4022636	2209	9.7	7.5	657	CSM
IES-007	Grapevine Spring	3/14/16	587257	4035099	1359	19.8	8.0	665	MH
IES-008	Grapevine Spring 2	3/14/16	587205	4035115	1360	17.2	7.8	926	MH
IES-052	Peak Spring	7/06/17	617004	4013692	3176	4*	7.9	202	CSM
IES-063	La Madre Spring	5/24/18	634277	4005801	1761	13.8	7.7	610	KST
IES-064	Willow Creek Spring	5/24/18	610794	4030910	1827	11.9	7.6	436	CSM
IES-065	Red Spring	7/27/18	642103	4001111	1117	20*	7.7	431	KST

Two major thrust faults separate the three primary rock regions (Fig. 2). The Keystone Thrust Fault, located in the southeastern Spring Mountains, occurs at the contact between the Aztec Sandstone (Ja) and the Bonanza King Dolostone (Cbk). There, Permian and Cambrian dolostone and limestone are thrust atop Mesozoic sandstones. The Wheeler Pass Thrust Fault, located in the northwest Spring Mountains, places the Stirling Quartzite (Zs) atop the Bird Springs Formation (Pmb) and marks the stratigraphic transition from Permian carbonate to Cambrian and Precambrian siliciclastic rocks. Similarly, numerous thrust faults such as the Lee Canyon Thrust, cut the CSM but do not displace different rock types.

3. Methods

Observations from geologic maps were combined with strontium isotopes and spring geochemistry and water isotope data to predict groundwater flowpaths for twelve springs and to infer groundwater flow in the rest of the Spring Mountains. Geologic structures are important controls on groundwater flow both within the DVRFS (Al-Qudah et al., 2017; Belcher and Sweetkind, 2010; D'Agnese et al., 1998) and globally (Dimmen et al., 2017; Seymour et al., 2008; Vittecoq et al., 2015). In fact, DVRFS spring emergences are highly correlated to structural features. Geologic maps (Page et al., 2005; Workman et al., 2016) were used to identify structural features and changes in rock types. Springs along pervasive thrust faults in the Spring Mountains were used to study how groundwater composition evolves along thrust faults and differs between regions. In addition, potentiometric surface maps displayed on Fig. 1 (D'Agnese et al., 1998) were used to infer groundwater flow direction.

Dissolved strontium and strontium isotope ratios (87Sr/86Sr), along with general geochemistry are commonly used to better understand potential groundwater flowpaths (Blum et al., 1993; Clow et al., 1997; Négrel et al., 2018; Pacheco and Van der Weijden, 2014b; Pu et al., 2012; Stevenson et al., 2018; Stewart-Maddox et al., 2018; Zieliński et al., 2017). As water flows through rocks and soils it accumulates dissolved strontium. The ⁸⁷Sr/⁸⁶Sr of the resulting water is a product of the initial ⁸⁷Sr/⁸⁶Sr of the water and the ⁸⁷Sr/⁸⁶Sr of material weathered along the flowpath. Differences in 87Sr/86Sr can be attributed to exposure to different mineral sources or to mixing between multiple water types if sources with distinguishable 87Sr/86Sr exist. Derivation of flowpaths from ⁸⁷Sr/⁸⁶Sr is limited by the extent of known ⁸⁷Sr/⁸⁶Sr in potential flowpath geology (Paces et al., 2007). We used published ⁸⁷Sr/⁸⁶Sr values from Spring Mountains units, the strontium sea water curve and rock age, and leaching experiments from outcrop samples to better constrain the range of potential 87Sr/86Sr and predict groundwater flowpaths.

Spring geochemistry can also be used to estimate weathering

patterns and to predict groundwater flowpaths (Blum et al., 1998; Garrels and Mackenzie, 1967; Johnson et al., 2000; Pretti and Stewart, 2002; Rademacher et al., 2001). Determining the amount of material weathered in carbonate and dolostone systems such as the Spring Mountains is difficult because calcite reaches saturation quickly and is easily precipitated. However, spring geochemistry can be used to identify the weathering of silicate minerals in addition to limestone (Blum et al., 1998; Jacobson et al., 2002). δ^{18} O and δ^{2} H can be used to estimate the fraction of recharge from snow and to identify different recharge elevations. (Beria et al., 2018; Penna et al., 2014; Winograd et al., 1998). We used δ^{18} O and δ^{2} H to better constrain potential flowpaths inferred from 87 Sr/ 86 Sr and spring geochemistry.

3.1. Sampling procedures and analyses

Spring water samples were collected from eight Spring Mountains springs in March of 2016. Four additional springs were added to increase spatial resolution in July 2017, May 2018, and July 2018. Samples were collected using a GeoTech peristaltic pump with Masterflex platinum-cured silicone tubing positioned at the spring source or uppermost discharge location. Field temperature measurements were collected at each spring source, whereas pH and conductivity were determined at the New Mexico Bureau of Geology & Mineral Resources Analytical Chemistry Laboratory (Table 1). At each spring, samples for cation and anion analysis were filtered with 0.22 μ m polyethersulfone membrane Sterivex-GP pressure filters and collected in 250 mL high density polyethylene bottles (HDPE). Water to be analyzed for 87 Sr/ 86 Sr was filtered and collected in 125 mL HDPE bottles. Water δ^{18} O and δ^{2} H samples were collected in 2 mL glass vials with no head space.

General chemistry and $\delta^{18}O$ and $\delta^{2}H$ samples were stored cold), and all samples were shipped to an analytical lab within six months. Strontium isotope samples were analyzed at University of Illinois, Urbana Champaign using a Nu Plasma HR multicollector inductively-coupled-plasma mass-spectrometer. Stable isotope samples were analyzed at the University of California, Davis stable isotope facility for $\delta^{18}O$ and $\delta^{2}H$ using a continuous flow isotope mass spectrometer. Major cations were measured using an ICP-OES according to EPA method 200.7 and major anions were measured using an IC according to EPA method 300.0 at the New Mexico Bureau of Geology & Mineral Resources Analytical Chemistry Laboratory. General chemistry, $^{87}\text{Sr}/^{86}\text{Sr}$, and water $\delta^{18}O$ and $\delta^{2}H$ values are reported in Table 2.

3.2. Rock leaching experiments & ⁸⁷Sr/⁸⁶Sr as a geochemical tracer

Rock 87 Sr/ 86 Sr were collected throughout the Spring Mountains and compared to groundwater 87 Sr/ 86 Sr to better understand rock

Mountains spring geochemistry and isotope values. ND = not detected. The detection limit for [Cl⁻] is 1 mgL⁻¹ or 2.8 × 10⁻² mmolL⁻¹. *Refer to Section 3.3, Eq. (1) for explanation of calculation.

EF-OR 1.25E - 03 2.06E - 03 2.17E - 03 5.71E - 05 1.04E - 02 8.19E - 02 1.78E - 03 1.78E - 03 4.5e - 5 4.083 4.00R ES-O01 2.029 0.779 0.048 0.002 0.330 0.611 9.178 0.794 1.48 0.71040 -8.6. -12.08 19 ES-002 1.299 0.779 0.031 0.001 0.0141 0.103 6.179 0.360 1.47 0.71038 -8.7.7 -12.13 2.2 ES-002 1.290 1.893 0.031 0.001 0.0141 0.103 6.179 0.736 0.739 0.71044 -9.29 -12.13 2.1 ES-002 1.296 1.296 0.031 0.001 0.014 0.355 0.735 0.739	ES Number Ca ²⁺ (mmo	$1 L^{-1}$	${ m Mg}^{2+}$ (mmol L ⁻¹)	Na ⁺ (mmol L ⁻¹)	K^+ (mmol L^{-1})) Sr ²⁺ (µmol L ⁻¹)	Cl^- (mmol L^{-1}) SO_4^{2-} (mmo	() SO_4^{2-} (mmol L ⁻¹)	$\mathrm{HCO_{3}}^{-}$ (mmol L^{-1})	Si (mmolL ⁻¹)	Si (mmol L ⁻¹) Mg ²⁺ /Ca ²⁺ (mol/mol)	87Sr/86Sr	δD ‰	⁸⁷ Sr/ ⁸⁶ Sr
2.029 2.995 0.779 0.048 0.002 0.330 0.611 9.178 0.794 1.48 0.71040 -86.6 -12.08 1.290 1.893 0.239 0.031 0.014 0.135 6.179 0.360 1.47 0.71038 -8.77 -12.13 1.290 1.893 0.239 0.031 0.014 0.355 0.735 0.540 0.612 0.73 0.71038 -8.77 -12.13 1.946 1.424 0.792 0.019 0.014 0.355 0.735 0.540 0.664 0.73 0.7102 -9.29 -13.18 2.221 2.037 0.234 0.034 0.003 0.095 0.156 0.590 0.790 <th>Error</th> <th>1.25E-03</th> <th>2.06E-03</th> <th>2.17E-03</th> <th>1.28E-03</th> <th>5.71E-05</th> <th>2.82E-02</th> <th>1.04E-02</th> <th>8.19E-02</th> <th>1.78E-03</th> <th></th> <th>±5e-5</th> <th></th> <th></th>	Error	1.25E-03	2.06E-03	2.17E-03	1.28E-03	5.71E-05	2.82E-02	1.04E-02	8.19E-02	1.78E-03		±5e-5		
1.290 1.893 0.239 0.031 0.0141 0.103 6.179 0.360 1.47 0.71038 -87.7 -12.13 1.946 1.424 0.792 0.019 0.014 0.355 0.735 5.540 0.612 0.73 0.70844 -92.9 -13.18 2.221 2.037 0.039 0.031 0.089 0.143 0.891 6.654 0.466 0.92 0.70841 -92.9 -13.18 1.462 1.432 0.033 0.031 0.008 0.143 0.891 6.654 0.466 0.92 0.70831 -93.5 -13.31 1.462 1.432 0.034 0.034 0.035 0.049 0.789 0.599 0.789 0.799 0.799 0.791 -13.75 1.417 1.621 1.079 0.044 0.085 0.049 2.799 0.773 1.31 9.2.1 1.31 0.751 0.256 0.079 0.079 0.049 0.799 0.779 0.798	IES-001	2.029	2.995	0.779	0.048	0.002	0.330	0.611	9.178	0.794	1.48	0.71040	-86.6	
1.946 1.424 0.792 0.019 0.014 0.355 0.735 5.540 0.612 0.73 0.70844 -92.9 -13.18 2.221 2.037 0.303 0.031 0.008 0.143 0.891 6.654 0.466 0.92 0.70831 -93.5 -13.18 1.462 1.432 0.234 0.034 0.005 0.156 5.507 0.509 0.709 0.7102 -95.2 -13.45 2.188 1.395 0.035 0.044 0.185 0.049 0.709 0.799 0.719 0.7102 -95.2 -13.45 1.417 1.621 1.079 0.044 0.049 2.049 0.719 1.14 0.7398 0.7308 0.91 -13.75 2.288 2.362 1.039 0.044 0.490 0.773 1.03 0.70879 -91.2 1.31 0.751 0.751 0.050 0.009 0.044 0.79 0.719 0.710 0.710 0.711 0.711	IES-002	1.290	1.893	0.239	0.031	0.001	0.141	0.103	6.179	0.360	1.47	0.71038		
2.221 2.037 0.303 0.031 0.008 0.143 0.891 6.654 0.466 0.92 0.70831 -93.5 -13.31 1.462 1.432 0.234 0.034 0.095 0.156 5.507 0.509 0.98 0.71102 -95.2 -13.45 2.188 1.395 0.025 0.044 0.185 0.089 7.080 0.580 0.64 0.70879 -99.1 -13.71 1.417 1.621 1.079 0.044 0.089 7.080 0.719 1.14 0.73344 -92.2 -13.15 2.288 2.362 1.624 0.049 2.499 4.900 0.773 1.03 0.73086 -91.9 -13.10 0.751 0.752 0.039 0.044 0.049 2.499 4.900 0.773 1.03 0.13 0.13 0.13 0.13 0.13 0.13 0.13 0.13 0.13 0.13 0.13 0.13 0.13 0.13 0.13 0.14 0.0	IES-003	1.946	1.424	0.792	0.019	0.014	0.355	0.735	5.540	0.612	0.73	0.70844		-13.18 77
1.462 1.432 0.234 0.034 0.095 0.156 5.507 0.509 0.89 0.71102 -95. -13.45 2.188 1.395 0.352 0.025 0.004 0.185 0.089 7.080 0.580 0.64 0.70879 -99.1 -13.71 1.417 1.621 1.079 0.044 0.089 7.080 0.739 0.7334 -92.2 -13.75 1.417 1.621 1.079 0.044 0.049 2.499 4.310 0.773 1.03 0.7334 -92.2 -13.15 2.288 2.362 0.052 0.009 0.494 2.499 4.900 0.773 1.03 0.70386 -91.9 -13.69 2.288 0.352 0.037 0.001 ND 0.027 2.114 0.128 0.7084 -91.9 -13.69 2.055 0.036 0.044 0.136 0.036 0.044 0.136 0.7084 -98.0 -12.74 1.242 0.745	IES-004	2.221	2.037	0.303	0.031	0.008	0.143	0.891	6.654	0.466	0.92	0.70831		-13.31 84
2.188 1.395 0.352 0.025 0.044 0.185 0.089 7.080 0.580 0.64 0.70879 -99.1 -13.71 1.417 1.621 1.079 0.044 0.008 0.417 1.239 4.310 0.719 1.14 0.73314 -92.2 -13.15 2.288 2.382 1.344 0.052 0.009 0.494 2.499 4.900 0.773 1.03 0.77384 -92.2 -13.15 0.751 0.295 0.037 0.016 0.001 0.005 0.085 0.207 6.736 0.477 0.679 0.7115 -92.4 -12.74 1.524 0.745 0.748 0.749 4.704 0.736 0.7115 -92.4 -12.74 1.529 0.745 0.748 0.049 0.044 0.136 4.704 0.67 0.7115 -92.4 -12.74 1.529 0.745 0.748 0.044 0.136 0.749 0.749 0.749 0.749 0.748	IES-005	1.462	1.432	0.234	0.034	0.003	0.095	0.156	5.507	0.509	0.98	0.71102	-95.2	
1.417 1.621 1.079 0.044 0.008 0.417 1.239 4.310 0.719 1.14 0.73314 -92.2 -13.15 2.288 2.362 1.344 0.052 0.009 0.494 2.499 4.900 0.773 1.03 0.73384 -92.2 -13.15 0.751 0.255 0.030 0.007 0.001 ND 0.027 2.114 0.128 0.738 -91.0 -13.10 2.053 0.378 0.016 0.001 0.005 0.085 0.207 6.736 0.417 0.67 0.71115 -92.4 -12.74 1.524 0.748 0.044 0.136 4.704 0.43 0.48 0.7084 -98.0 -13.48 1.203 0.210 0.050 0.001 0.146 0.239 4.327 0.438 0.86 -98.7 12.06	IES-006	2.188	1.395	0.352	0.025	0.004	0.185	0.089	7.080	0.580	0.64	0.70879	-99.1	-13.71 105
2.288 2.362 1.344 0.052 0.009 0.494 2.499 4.900 0.773 1.03 0.73086 -919 -13.10 0.751 0.295 0.030 0.007 0.001 ND 0.027 2.114 0.128 0.39 0.70832 -96 -13.69 2.053 1.378 0.181 0.016 0.002 0.085 0.207 6.736 0.417 0.67 0.71115 -92.4 -12.74 1.542 0.745 0.745 0.014 0.005 0.044 0.136 4.704 0.300 0.48 0.70864 -98.0 -13.48 1.203 0.210 0.050 0.001 0.146 0.239 4.327 0.438 0.86 - -88.7 -12.06	IES-007	1.417	1.621	1.079	0.044	0.008	0.417	1.239	4.310	0.719	1.14	0.73314	-92.2	
0.751 0.295 0.030 0.007 0.001 ND 0.027 2.14 0.128 0.39 0.70832 -96.0 -13.69 2.053 1.378 0.181 0.016 0.002 0.085 0.207 6.736 0.417 0.67 0.71115 -9.24 -12.74 1.542 0.745 0.745 0.016 0.005 0.044 0.136 4.704 0.300 0.48 0.70864 -9.80 -13.48 1.203 0.210 0.050 0.001 0.146 0.239 4.327 0.438 0.86 - -8.87 -12.06	IES-008	2.288	2.362	1.344	0.052	0.009	0.494	2.499	4.900	0.773	1.03	0.73086		-13.10 73
2.053 1.378 0.181 0.016 0.002 0.085 0.207 6.736 0.417 0.67 0.71115 -92.4 -12.74 1.542 0.745 0.102 0.014 0.005 0.044 0.136 4.704 0.300 0.48 0.70864 -98.0 -13.48 1.203 0.210 0.050 0.001 0.146 0.239 4.327 0.438 0.86 - -88.7 -12.06	IES-052	0.751	0.295	0.030	0.007	0.001	ND	0.027	2.114	0.128	0.39	0.70832		-13.69 104
$\begin{array}{cccccccccccccccccccccccccccccccccccc$	IES-063	2.053	1.378	0.181	0.016	0.002	0.085	0.207	6.736	0.417	0.67	0.71115		-12.74 54
1.203 1.029 0.210 0.050 0.001 0.146 0.239 4.327 0.438 0.8688.7 -12.06	IES-064	1.542	0.745	0.102	0.014	0.005	0.044	0.136	4.704	0.300	0.48	0.70864	-98.0	
	IES-065	1.203	1.029	0.210	0.050	0.001	0.146	0.239	4.327	0.438	0.86	ı	-88.7	

weathering and groundwater flowpaths. However, prior to this study, only a subset of rocks present in the Spring Mountains had published ⁸⁷Sr/⁸⁶Sr values (Paces et al., 2007). To fill this gap, eighteen total rock samples were selected from sixteen geologic units hypothesized to be significant to groundwater flow based on published cross sections (Page et al., 2005) and DVRFS characterization (Belcher and Sweetkind, 2010). Rock samples were collected from outcrops in the Spring Mountains in March 2018. Geologic maps by Page et al. (2005) and Workman et al. (2016) were used to determine sample locations for each of the sixteen units. Fresh rock samples typically about 1000 cm³ were collected from each outcrop.

⁸⁷Sr/⁸⁶Sr values were determined from leachate water using methods adapted from Frisbee et al. (2017). Rock samples were crushed and sieved with a 0.4 size sieve (4.76 mm) at Purdue University. For each geologic unit, 200 mg of crushed rock was added to a 1 L HDPE bottle with deionized water. The bottles were capped tightly, sealed with electrical tape, and stored for 2 months in the laboratory. After the allotted time, samples were decanted and analyzed at the ICMPS facility at University of Illinois – Urbana Champaign. Rock leaching results are reported with previously published ⁸⁷Sr/⁸⁶Sr values in Table 3.

Leaching with deionized water provides information on the most easily released sources of strontium in the host rocks. However, by crushing the rock we aim to increase the mineral surface area and enhance weathering of the more resistant minerals. One shortcoming of this technique is that water is essentially stagnant in the bottle unless the bottle is occasionally agitated and does not represent natural conditions where solutes are transported away from the mineral surface by flowing water. The Paces et al. (2007) methodology included powdering whole rocks and leaching them in dilute hydrochloric acid. These methods may give slightly different results since there is heterogeneity within the mineralogy of a rock sample and because hydrochloric acid aggressively weathers a broader assemblage of minerals compared to deionized water.

3.3. Spring Mountains recharge

Spring water $\delta^{18}O$ values were utilized to determine the relative importance of snow and rain to groundwater recharge in the study area (Genereux, 1998; Liu et al., 2004; Winograd et al., 1998). δ^{18} O values of rain and snow reported in Winograd et al. (1998) were used to create a weighted average for each precipitation type. The calculation only sourced δ¹⁸O from Winograd et al. (1998) because other Spring Mountains stable isotope studies do not report amount of precipitation for each $\delta^{18}\text{O}$ observation. The fraction of recharge from snow was computed using Eq. (1), where $\delta^{18}O_{Spring}$ is the measured $\delta^{18}O$ value for spring water, $\delta^{18}O_{Rain}$ is the weighted mean of rain $\delta^{18}O$ observations, and $\delta^{18}O_{Snow}$ is the weighted mean of snow $\delta^{18}O$ observations from 88 observations of rain (n = 41) or snow (n = 47) collected between 1975 and 1978 and 1987 to 1988 (Winograd et al., 1998). Eq. (1) is a twoendmember mixing model that assumes $\delta^{18}O$ of snowmelt and rainfall are the only sources of $\delta^{18}O$ influencing discharging groundwater (Beria et al., 2018; Penna et al., 2014; Winograd et al., 1998).

$$f_{snow} = \frac{\delta^{18} O_{Spring} - \delta^{18} O_{Rain}}{\delta^{18} O_{snow} - \delta^{18} O_{rain}}$$

$$\tag{1}$$

The certainty of the calculated fraction of recharge from snow is limited by the incomplete precipitation record throughout a non-consecutive six year period (Winograd et al., 1998), which may bias endmembers. Isotopes of precipitation vary from storm to storm and from year to year (Dansgaard, 1964), thus increasing the potential for uncertainty due to the incomplete precipitation record. In addition, rain data were collected at three locations and snow data were collected at five locations, limiting the spatial coverage of the record. Discharging spring water is likely not fully represented by recharge during the six years that data are available. For example, Springer et al. (2016)

Table 3⁸⁷Sr/⁸⁶Sr from IES rock leaching experiments and Paces et al. (2007). Comparison of Paces et al., (2007) and IES data is presented in Fig. 3. Map color corresponds with Fig. 1. Individual rock units were grouped into three colors as determined by geologic age, composition, and ⁸⁷Sr/⁸⁶Sr. The map color for each rock unit is listed under Map Color and corresponds to Fig. 1. Flow group #1 is the Keystone Thrust flow region; flow group #2 is the central Spring Mountains flow region; flow group #3 is the Montgomery Hills flow region.

Rock Unit	Rock Unit Name	Map Color	Hand Sample	Present in Flow	Rock Lea	aching Expe	riments		Paces et al., (2007) ⁸⁷ Sr/ ⁸⁶ Sr
Symbol			Composition	Group	Easting	Northing	⁸⁷ Sr/ ⁸⁶ Sr	Uncertainty	 range
Ja	Aztec Sandstone	Green	Sandstone	1	636589	3986128	0.71116	±0.00005	_
JTrKc	Kayenta Formation	Green	Sandstone	1	638579	3984572	0.71115	± 0.00005	-
JTrKc	Kayenta Formation	Green	Conglomerate	1	638594	3984548	0.71102	± 0.00005	_
Trml	Lower Moenkopi Formation	Green	Limestone	1,2	640941	3992477	0.70827	±0.00005	-
Pkt	Kaibab and Toroweap Formations	Purple	Limestone	1	644610	3990660	0.70829	±0.00005	-
Pr	Lower Permian Redbeds	Purple	Sandstone	1,2	644810	3990706	0.70823	± 0.00005	-
Pmb	Bird Springs Formation	Purple	Limestone	1,2,3	632669	3987605	0.70875	± 0.00005	0.70790-0.70913
Mm	Monte Cristo Group	Purple	Limestone	1,2,3	633411	3987535	0.70836	± 0.00005	0.70844
Mdu	Mississippian and Devonian Rocks	Purple	Limestone	1,2,3	634119	3987346	0.70855	±0.00005	0.70862-0.70886
Dsi	Simonson Dolostone	Purple	Dolostone	2	_	_	_	_	0.70862-0.70866
Dsu	Devonian & Silurian Rocks undivided	Purple	Dolostone	2	-	-	-	-	-
DOm	Mountain Springs Formation	Purple	Dolostone	1,2	634735	3988093	0.70891	±0.00008	-
Oes	Ely Springs Dolostone	Purple	Dolostone	2	-	_	-	_	0.70813-0.70946
Oe	Eureka Quartzite	Purple	Quartzite	2	-	-	-	_	-
Ocp	Pogonip Group	Purple	Quartzite	2,3	582066	4024796	0.71200	± 0.00005	0.71200
Cn	Nopah Formation	Purple	Dolostone	1,2,3	634957	3988110	0.70898	± 0.0001	0.70847-0.71013
Cbk	Bonanza King Formation	Purple	Dolostone	1,2,3	635150	3988220	0.70935	± 0.0001	0.70857-0.72543
Cbk	Bonanza King Formation	Purple	Dolostone	1,2,3	585382	4034067	0.71235	± 0.00005	0.70857-0.72543
Cc	Carrara Formation	Yellow	Limestone	3	585245	4034444	0.71315	± 0.00005	0.71018-0.71282
Cz	Zabrinskie Quartzite	Yellow	Quartzite	3	585113	4034417	0.72237	± 0.00005	_
Czw	Wood Canyon Formation	Yellow	Quartzite	3	583433	4034253	0.71205	± 0.00005	0.70945-0.72543
Zs	Stirling Quartzite	Yellow	Quartzite	3	-	-	-	_	0.71125-0.71343
Zj	Johnnie Quartzite	Yellow	Quartzite	3	581158	4033515	0.71136	±0.00005	-

reported stable isotope samples collected from 2011 to 2012 for many of the same springs sampled by Hershey (1989) from 1985 to 1987, which are on average 0.61% greater for $\delta^{18}O$ and 1.34% greater for $\delta^{2}H$ 24–27 years later. Uncertainty in the fraction of recharge from snow is further increased by the limited spatial extent of sample collection. Instances of percent snow values greater than 100% are likely due to spatiotemporal limitations of the record used to define endmembers.

4. Results

4.1. Stable isotope observations

Spring water $\delta^{18}O$ and $\delta^{2}H$ range from -12.06 to $-13.71 \pm 0.08\%$ and -86.6 to $-99.1 \pm 0.83\%$, respectively (Table 2, Fig. 3). Winograd et al. (1998) and Hershey (1989) collected rain and snow within the Spring Mountains for multiple seasons between 1975 and 1988, and our spring water $\delta^{18}O$ and $\delta^{2}H$ values fall

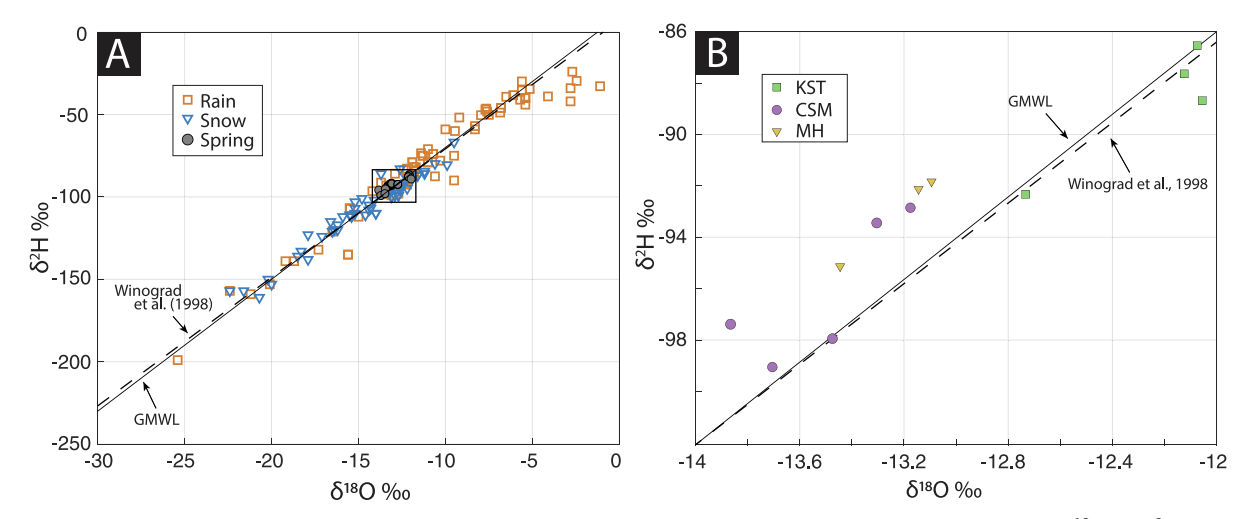


Fig. 3. A) Stable isotope plot of Spring Mountains Springs (gray circles) and published rain (orange squares) and snow (blue triangles) $\delta^{18}O$ and δ^2H values (Hershey, 1989; Winograd et al., 1998). The global meteoric (GMWL), $\delta D = 8\delta^{18}O + 10$ is plotted in black. The local meteoric water line from Winograd et al. (1998), $\delta D = 7.8\delta^{18}O + 7.2$ is plotted as a dashed black line. 3B) Zoomed in view of Fig. 3A focusing on sampled springs. Water lines, rain, and snow points are styled in the same manner as Fig. 3A. Springs are colored by flow region with green = KST, purple = CSM, yellow = MH. (For interpretation of the references to color in this figure legend, the reader is referred to the web version of this article.)

within the historical range for those studies (Fig. 3). δ^{18} O values of rain and snow reported in Winograd et al. (1998) were used to calculate a weighted average δ^{18} O for rain and snow, and were combined with spring water δ^{18} O values in Eq. (1) to calculate the percentage of recharge from snow for each spring. The percentage of snow contributing to spring recharge ranges from 18 to 105 % (Table 2). This estimate is limited by the unevenly distributed data over the 6-year period of record.

Springs emerging along the KST have δ^{18} O and δ^{2} H values ranging between -12.74 and $-12.06 \pm 0.08\%$ and -92.4% and $-86.6\% \pm 0.83\%$, respectively. KST springs are isotopically heavier than the rest of sampled springs and receive between 18 and 54% of their recharge from snow based on 2 end-member mixing calculations using snow and rainfall δ^{18} O data from Winograd et al. (1998). Springs discharging in the CSM emerge at the highest elevations in the Spring Mountains and have relatively lighter $\delta^{18}O$ and $\delta^{2}H$, ranging between -13.71and $-13.18 \pm 0.08\%$ and -99.1.4% $-92.9\% \pm 0.83\%$, respectively. CSM springs receive more than 77% of their recharge from snow based on mixing analysis using δ^{18} O precipitation data from Winograd et al. (1998). Springs in the MH flow region have intermediate δ^{18} O and δ^{2} H, ranging between -13.45 and $-13.1 \pm 0.08\%$ and -95.2% and $-91.9\% \pm 0.83\%$, respectively. MH springs receive between 73 and 91% of their recharge from snow based on δ^{18} O precipitation data from Winograd et al. (1998).

4.2. Spring geochemistry

Sampled spring waters were grouped according to their hydrochemical facies. All springs in the study area are either $Ca-HCO_3^-$ or $Mg-HCO_3^-$ water (Fig. 4) and are saturated with respect to calcite and dolomite. Generally, the degree of saturation with respect to calcite and dolomite increases from the CSM to MH to KST. Springs in this study exhibit a positive correlation between $Ca^{2+} + Mg^{2+}$ and $SO_4^{2-} + \frac{1}{2}$ HCO_3^- , and follow the expected geochemical trend for dedolomitization as distance from the recharge area increases (Fig. 5, R2 = 0.989) (Raines and Dewers, 1997). Dedolomitization occurs as groundwater weathers dolomite and gypsum (50:50) and subsequently supersaturates groundwater with calcite (Raines and Dewers, 1997).

The Mg^{2+}/Ca^{2+} of spring waters varies from 0.39 to 1.48 throughout the Spring Mountains. High Mg^{2+}/Ca^{2+} (>1) is more

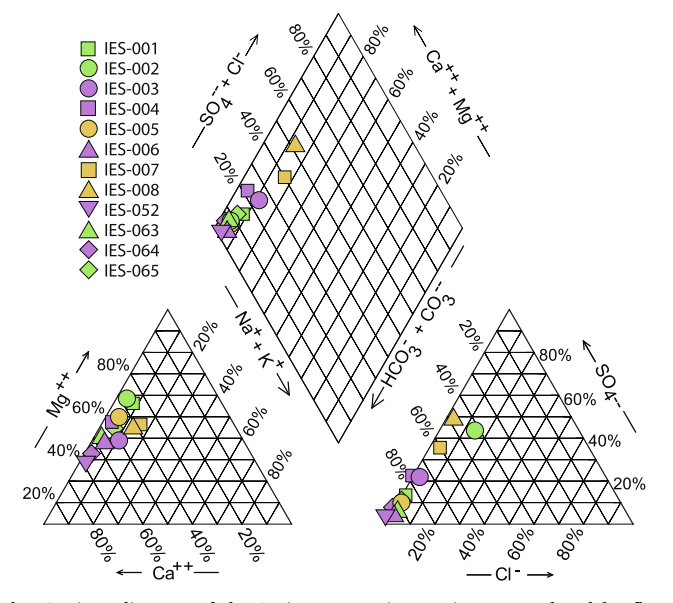


Fig. 4. Piper diagram of the Spring Mountains. Springs are colored by flow region with green = KST, purple = CSM, yellow = MH. (For interpretation of the references to color in this figure legend, the reader is referred to the web version of this article.)

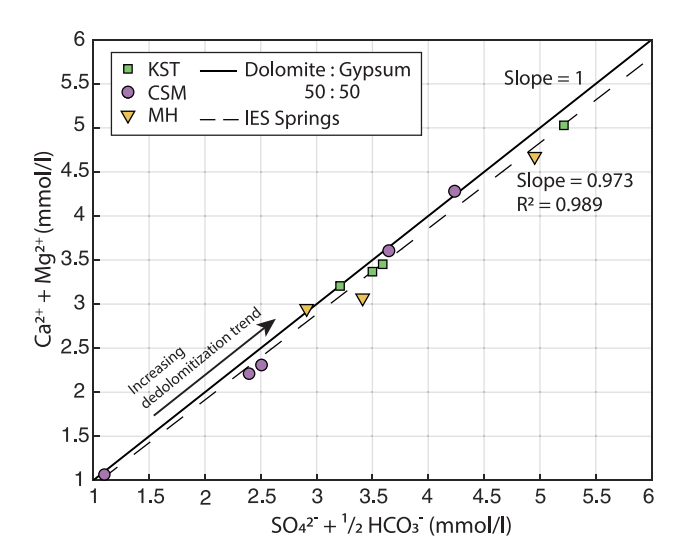


Fig. 5. Plot showing dedolomitization trend in Spring Mountains groundwater. The solid line represents 1:1 weathering between dolomite and gypsum, data along this trend indicate increasing dedolomization (Raines and Dewers, 1997). Springs are colored by flow region with green = KST, purple = CSM, yellow = MH. (For interpretation of the references to color in this figure legend, the reader is referred to the web version of this article.)

commonly observed in springs discharging at lower elevations (below 1700 m) and in springs with relatively warmer temperatures ($>15\,^{\circ}\text{C}$). Springs discharging along the KST in the southern Spring Mountains near Mountain Springs, NV (IES-001 and IES-002, Fig. 1) emerge from dolostone (Bonanza King and Nopah Formations) and exhibit very high $\text{Mg}^{2+}/\text{Ca}^{2+}$; 1.48 and 1.47, respectively. Springs discharging along the northern portion of the KST near Red Rock Canyon National Conservation Area (IES-063 and IES-065) have lower $\text{Mg}^{2+}/\text{Ca}^{2+}$, 0.67 and 0.86, respectively. $\text{Mg}^{2+}/\text{Ca}^{2+}$ in CSM springs ranges from 0.39–0.92 and 0.89–1.14 in the MH. Spring temperature and $\text{Mg}^{2+}/\text{Ca}^{2+}$ are

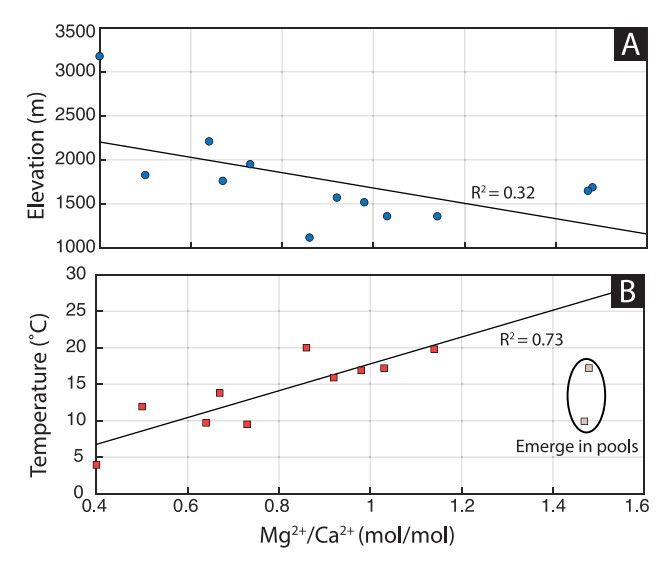


Fig. 6. Plot comparing temperature and elevation to ${\rm Mg^{2+}/Ca^{2+}}$. Temperatures for IES-052 and IES-065 were not collected during field sampling and were supplemented with USGS data (USGS 361541115415001 and USGS 360840115251001, respectively) (USGS, 2019). IES-001 and IES-002 (light red) emerge in shallow pools with low discharge (>1 L/s). The pool temperature is influenced by the temperature of the atmosphere and is not representative of the discharging groundwater. IES-001 and IES-002 were not used in the temperature versus ${\rm Mg^{2+}/Ca^{2+}}$ regression line and ${\rm R^2}$ calculation for this reason. (For interpretation of the references to color in this figure legend, the reader is referred to the web version of this article.)

positively correlated ($R^2 = 0.74$, Fig. 6B). IES-001 & IES-002 are not included in the temperature relationship as they discharge in low-flow pools and have significant diurnal temperature signals. The diurnal temperature signal was observed using a long-term temperature logger with a sampling interval of 15 min in IES-002. Although IES-001 did not have a logger in place, it likely also exhibits diurnal temperature fluctuations because of the very low discharge (>1 L s⁻¹) in a shallow pool.

4.3. Strontium spring water and rock leaching experiment results

Spring water $^{87} Sr/^{86} Sr$ range from 0.70831 to 0.73314 \pm 0.00005 (Table 2). Springs near the KST include IES-001, 002, 063 and 065, and their $^{87} Sr/^{86} Sr$ range between 0.71038 and 0.71115 \pm 0.00005 ($^{87} Sr/^{86} Sr$ data is not available for IES-065 at this time). Springs in the CSM include IES-003, 004, 006, 052, and 064, and have the lowest $^{87} Sr/^{86} Sr$ of all measured springs (0.70831–0.70879 \pm 0.00005). Springs in the MH (or northwest of the Wheeler Pass Thrust Fault) include IES-005, 007, and 008 and have a $^{87} Sr/^{86} Sr$ of 0.71102–0.73314 \pm 0.00005, the highest of all measured springs.

Rock leaching 87 Sr/ 86 Sr range from 0.70823 to 0.72237 \pm 0.00005 (Table 3). We did not conduct leaching experiments on five units present in the Spring Mountains (Table 3) because the units are thin (Dsi, Dsu, Oe, Oes) or only observed in the MH (Zs). 87 Sr/ 86 Sr for these five units was supplemented by 87 Sr/ 86 Sr values from (Paces et al., 2007). Paces et al. (2007) conducted multiple rock leaching experiments on rocks collected throughout southern Nevada for many of the geologic units present in the Spring Mountains. Many of the rock leaching 87 Sr/ 86 Sr reported in Paces et al. (2007) were collected from outcrops containing units present in the Spring Mountains but were collected outside of the Spring Mountains in other areas of southern Nevada. 87 Sr/ 86 Sr from rock leaching experiments in our study are within the range of previously published rock leaching data for the same geologic units in the region (Fig. 7, Table 3).

Groundwater $^{87}\rm{Sr}/^{86}\rm{Sr}$ was compared to nearby rocks using the $^{87}\rm{Sr}/^{86}\rm{Sr}$ results from rock leaching experiments on Spring Mountains

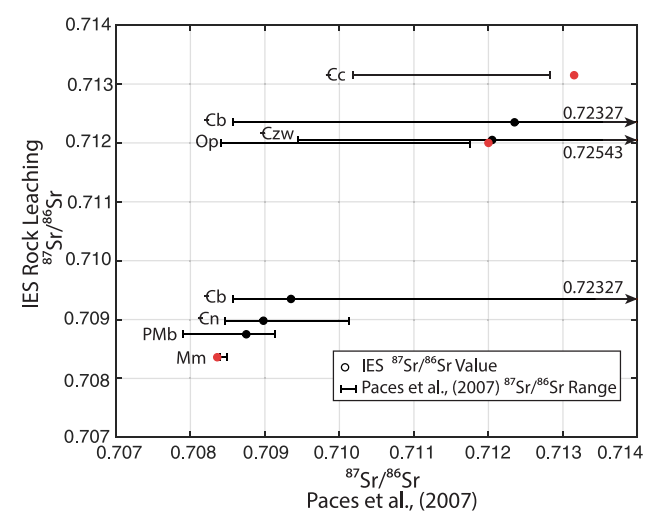


Fig. 7. Plot comparing IES rock leaching results to rock leaching results in Paces et al. (2007). IES rocks were crushed and leached in deionized water for 2 months. Paces et al. (2007) powdered and leached rocks in HCl. IES data are plotted with the same x and y value as black circles. Paces et al. (2007) data for the same rock unit is plotted along the x axis as a bar representing the range of Paces et al. (2007) data, the y value for the bars is the IES rock leaching $^{87}\text{Sr}/^{86}\text{Sr}$ for a given rock unit. IES data displayed in red do not fall in the range of Paces et al. (2007). Generally, agreement between leaching methods is good. Samples are labeled with their rock abbreviation (Table 3) directly to the left of the low value for the Paces et al., (2007) range. (For interpretation of the references to color in this figure legend, the reader is referred to the web version of this article.)

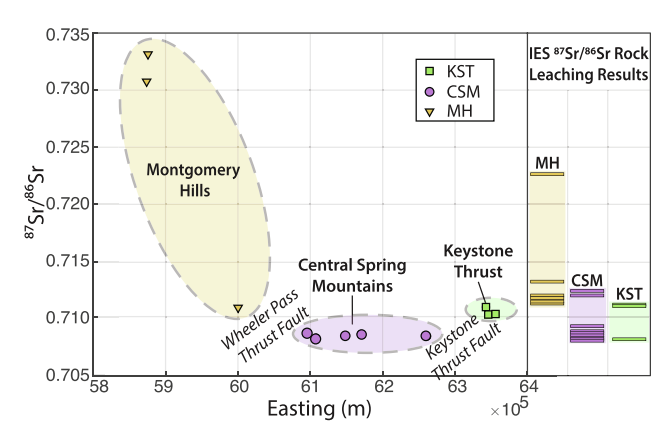


Fig. 8. Plot showing groundwater flow regions. The Keystone Thrust flow region is green, the Central Spring Mountains flow region is purple, and the Montgomery Hills flow region is yellow. Flow regions are separated by two major thrust faults, the Keystone Thrust and the Wheeler Pass Thrust (both trend northeast-southwest). Springs near the KST have ⁸⁷Sr/⁸⁶Sr of ~0.71. CSM springs have ⁸⁷Sr/⁸⁶Sr of ~0.708. Springs in the MH have ⁸⁷Sr/⁸⁶Sr greater than 0.71. Rock leaching results are displayed as colored bands on the left y axis. Green bands correspond with sandstones sampled in the KST. Purple bands are dolostone and limestone present in the CSM. Yellow bands display rocks in the MH. (For interpretation of the references to color in this figure legend, the reader is referred to the web version of this article.)

rocks. The footwall of the KST comprises a sequence of Mesozoic sandstones, whereas the hanging wall is limestone and dolostone. Mesozoic sandstones in the footwall are the only rocks with ⁸⁷Sr/⁸⁶Sr greater than 0.710 present in the potential flowpaths of KST springs (based on D'Agnese et al., 1998). Rocks in the hanging wall of the KST have $^{87}\text{Sr}/^{86}\text{Sr}$ of 0.70836–0.70935 \pm 0.00005. Rocks in the CSM are predominately younger limestone units atop older dolostone; however thin quartzite beds are also rarely present. Dolostone and limestone 87 Sr/ 86 Sr in the CSM range between 0.70823 and 0.71200 \pm 0.00005. Only three (Bonanza King Formation, Nopah Formation, and the Pogonip Group) of fourteen CSM units are greater than 0.70898. 87Sr/86Sr of rocks in Montgomery Hills (0.71136-0.72237 \pm 0.00005) are the highest ${}^{87}\mathrm{Sr}/{}^{86}\mathrm{Sr}$ in the region for both rocks and water. Diagenetic fluids that previously circulated through rubidium-rich rocks and deposited radiogenic strontium are likely the cause of the elevated ⁸⁷Sr/⁸⁶Sr present in the region (Paces et al., 2007).

5. Discussion

Three distinct but connected flow regions exist in the Spring Mountains: the KST, the CSM, and the MH (Fig. 8). The identification of flow regions is supported by evidence from 1) δ^{18} O and δ^{2} H, 2) spring geochemistry, and 3) comparison 87 Sr/ 86 Sr from spring water and rock leaching experiments to Spring Mountains geology.

5.1. Recharge patterns

Spring water $\delta^{18}O$ and δ^2H in the Spring Mountains vary because of differences in the dominant recharge source (rain vs. snow). The sandstone cliffs in the footwall of the KST are at a lower elevation than Mt. Charleston and thus receive a greater proportion of rain. As a result, $\delta^{18}O$ and δ^2H of precipitation along the Wilson Cliffs (Fig. 1) is heavier than CSM precipitation based on modeled spatial variations in isotope values of precipitation across the United States (Bowen, 2019; Bowen and Revenaugh, 2003). KST springs IES-001, IES-002, and IES-065 receive between 18 and 22% of recharge from snow. KST springs (IES-063 is located at a higher elevation than the southern KST springs (IES-001, IES-002, and IES-065) and receives a greater proportion of recharge from snow (54%). The relatively light stable isotopic signature of IES-

S.R. Warix, et al. Journal of Hydrology 580 (2020) 124313

063 suggests that the La Madre Fault may be a conduit for groundwater flow that is recharged at high elevations in the CSM. Groundwater flows down-gradient from the CSM recharge area along the La Madre Fault before discharging at IES-063 (D'Agnese et al. 1998). Rain recharging the KST also contributes to flow at IES-063 but with a smaller contribution than to southern springs. The southern portion of the KST is at a lower elevation and potentiometric gradient, and thus groundwater present has a greater potential to accumulate flow derived from rain as KST flowpath length increases. Springs along the KST are recharged by both rain falling over the sandstone cliffs and by rain and snow that recharges through limestone and dolostone present at higher elevations in the CSM, with the fraction of recharge by rain in the southern KST.

CSM precipitation falls primarily as snow at high elevations, such as Mt. Charleston, but also receives some summer rain, as evident by the high fraction of recharge by snow (77–105% snowmelt) in discharging springs. Spring waters in the CSM are closest to $\delta^{18}O$ and δ^2H for historical snow observations compared to springs in the KST and MH (Hershey, 1989; Winograd et al., 1998) (Fig. 3). Potentiometric contours developed by D'Agnese et al. (1998) suggest that water recharged at high elevations around Mt. Charleston flows downgradient toward IES springs, thus suggesting a pathway for high fractions of snow recharge reaching springs at lower elevations.

MH $\delta^{18}O$ and $\delta^{2}H$ values suggest that MH groundwater is recharged by a mixture of rain in the MH and snow from the CSM. The fraction of recharge by snow (73–91%) implies that recharge is primarily sourced from CSM snow with a minor local recharge component from warmer (lower elevation) rains. As distance from the CSM increases, the ratio of recharge by rain increases. For example, IES-005 has the greatest proportion of recharge by snow (compared to IES-007 and -008), and is the closest spring to the CSM in the MH flow region.

5.2. Groundwater weathering patterns and flow depth

All springs in this study exhibit the geochemical signature expected for dedolomitization. The ratio of the concentrations of ${\rm Ca^{2}}^+ + {\rm Mg^{2}}^+$ to ${\rm SO_4}^{2-} + {\rm 1/2}$ HCO $_3^-$ of approximately one, which represents a 50:50 weathering of dolomite:gypsum (Fig. 5) (Raines and Dewers, 1997). The positive correlation (slope = 0.927, ${\rm R^2} = 0.989$) between sampled spring geochemistry and the dedolomitization trend line suggests that all springs weather both dolomite and gypsum and subsequently precipitate calcite. Dolostone is not common in the MH or in the footwall of the KST but is found throughout the CSM, however, the dedolomitization signature is observed throughout all of the Spring Mountains which indicates a hydrologic connection from the CSM to the KST and MH.

Mg²⁺/Ca²⁺ can be used as a proxy for flow depth in the Spring Mountains because of the stratigraphic order of carbonates, typically dolostones are present at depth and limestones near the surface. Higher ratios of Mg²⁺/Ca²⁺ indicate deeper flow and lower ratios indicate shallower flow. Mg²⁺/Ca²⁺ values vary throughout the sampled Spring Mountains spring waters and are a function of both calcite precipitation and dolomite dissolution. As recharging waters weather shallow limestone, [Ca²⁺] increases. The water flows through deeper dolostones and continues to weather [Ca2+] and [Mg2+] until the water is saturated with respect to [Ca²⁺] and calcite precipitation begins. Generally, Mg²⁺/Ca²⁺ increases as spring elevation decreases because most high elevation springs emerge in limestone units that have limestone upgradient, thus limiting the possibility of significant flow through dolostone (Fig. 6A). Groundwater emerging at lower elevations likely travels through deeper dolostone before discharging at the surface, and thus has a higher Mg²⁺/Ca²⁺. The positive correlation between spring water temperature and Mg^{2+}/Ca^{2+} ($R^2 = 0.74$) suggests that springs with higher Mg²⁺/Ca²⁺ ratios may be sourced by groundwater from greater depths and/or were recharged by low elevation rain (rather than high elevation snow) (Fig. 6B).

Springs emerging along the KST have variable ${\rm Mg^{2+}/Ca^{2+}}$ (Table 2) as a result of differing amounts of limestone and dolostone weathering.

Springs with low ${\rm Mg^{2}}^{+}/{\rm Ca^{2}}^{+}$ around the KST are likely sourced by shallower flowpaths that have not passed through older and deeper dolostone. For example, IES-063 emerges in the Monte Cristo Group, a young limestone with no dolostones upgradient. In contrast, springs with high ${\rm Mg^{2}}^{+}/{\rm Ca^{2}}^{+}$ along the southwest and lower hydrologic gradient portion of the KST (IES-001 and IES-002) are interpreted as being sourced by deeper flowpaths that weather dolostone. These springs emerge in dolostones such as the Nopah and Bonanza King formations down-section of the Monte Cristo Group. It is difficult to use temperature as a proxy for circulation depth in the KST because many springs emerge in shallow pools with low discharge rates that are likely influenced by ambient air temperatures.

Mg²⁺/Ca²⁺ in CSM springs suggest that circulation depth in the CSM is variable. Springs with low Mg²⁺/Ca²⁺ are likely fed by predominantly by shallow flowpaths because upgradient CSM strata are limestone while older and deeper units are dolostone (Table 3). Variable flow depths by CSM groundwater are further supported by the relationship between spring temperature and Mg2+/Ca2+. For example, IES-052 ($Mg^{2+}/Ca^{2+} = 0.39$) emerges at high elevation on Mt. Charleston in the Bird Springs Formation (limestone) and has the lowest temperature (4 °C, USGS, 2019) of all sampled springs. No geologic unit is present upgradient of the Bird Springs Formation in the CSM indicating that limestone is the primary control on groundwater geochemistry for IES-052. In contrast, IES-004 $(Mg^{2+}/Ca^{2+} = 0.92)$ emerges in the Bonanza King Formation (dolomite) and has the highest spring water temperature (15.9 °C) in the CSM. Snowmelt recharges IES-004 then flows through limestone and deeper dolostone and warms before discharging at the surface. Typically, when groundwater is in contact with dolomite along the flowpath, Mg2+/Ca2+ is higher and circulation is deeper.

Mg²⁺/Ca²⁺ in the MH suggest that discharging groundwater has undergone deep circulation. All three MH springs have Mg²⁺/Ca²⁺ greater than 0.98 indicating significant calcite precipitation. Deep groundwater circulation is further suggested by spring water temperatures (16.9-19.8 °C), as MH spring waters are warmer than CSM groundwater because of warming by the geothermal gradient after deep circulation. However, using geothermometers is complicated in this study area because 1) Ca2+ and Mg2+ are not conservative such that Mg²⁺ concentrations increase and Ca²⁺ concentrations decrease as calcite is precipitated during dedolomitization, and 2) the mineralogy of the dolomitic rocks do not contain abundant (by volume) minerals containing silica, sodium, and potassium, thus Na-K-Ca and Si geothermometers do not provide meaningful estimates of the equilibrium temperature. We infer from Fig. 6b that circulation depth must increase since the temperature of spring waters increase as ${\rm Mg}^{2+}/{\rm Ca}^{2+}$ increases.

5.3. Groundwater flowpaths as inferred from ⁸⁷Sr/⁸⁶Sr and geology

87Sr/86Sr Springs emerging along the KST have a (0.71038-0.71116) higher than the limestone and dolostone east of Mt. Charleston that make up the hanging wall of the (0.70836–0.70935). The only sources of higher 87 Sr/ 86 Sr in nearby bedrock are the Aztec Sandstone (0.71116) and the Kayenta Formation (0.71102), and both of these units are present in the footwall of the KST. The Aztec Sandstone outcrops as massive sandstone cliffs to the east of sampled springs and is higher in elevation than KST spring emergence locations. In addition, the Aztec sandstone and its correlative equivalents have been documented to have high porosity in southeastern Nevada (Fossen et al., 2015) and in Utah (Beitler et al., 2005). Groundwater travels downgradient from north to south along the KST as it weathers Mesozoic sandstones in the hanging wall of the KST (Fig. 9). For example, IES-063 (1761 m) emerges around the northernmost point of the Wilson Cliffs (Fig. 1) at an elevation higher than other springs along the KST (IES-001, 1688 m; IES-002, 1648 m). The ⁸⁷Sr/⁸⁶Sr of IES-063 (0.71115) suggests that the spring is sourced

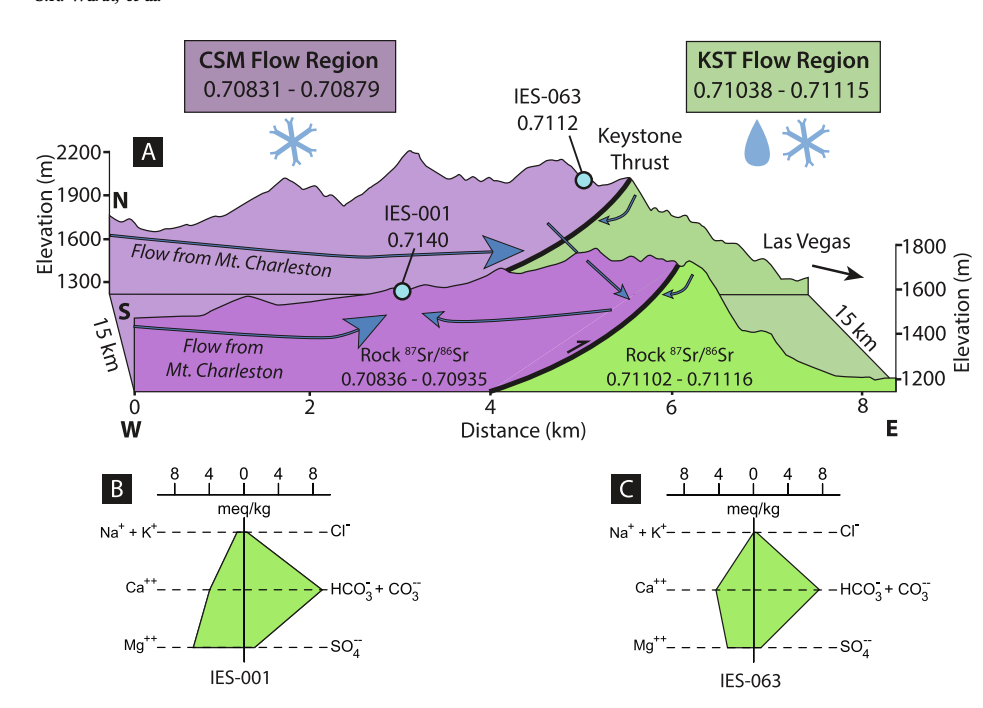


Fig. 9. A Conceptual diagram of flowpaths contributing to springs along the Keystone Thrust with IES-001 as a representative example, arrow size approximates contribution of flow. Each flow region heading displays the range of 87Sr/86Sr for spring water in the region, dominant recharge mechanism is displayed below each heading. Rocks displayed in green are sandstones, rocks displayed in purple are limestone and dolostone. Spring locations are approximate. The northern Keystone Thrust is higher in elevation than the southern Keystone Thrust. Groundwater emerging at IES-001 primarily weathers carbonate rocks as shown by the high concentrations of Ca²⁺, Mg²⁺, and HCO₃ in the stiff diagram but also has a $^{87}\mathrm{Sr}/^{86}\mathrm{Sr}$ that reflects sandstones to the east. Flow to IES-001 is sourced from two locations; 1) water flowing through dolostone and limestone that was recharged near Mt. Charleston, and 2) water flowing down-gradient along the Keystone Thrust after recharge on the sandstone cliffs. Fig. 9B. Stiff diagram of IES-001. Fig. 9C. Stiff diagram of IES-063. (For interpretation of the references to color in this figure legend, the reader is referred to the web version of this article.)

by flowpaths that originate in Mesozoic sandstone. As water flows through Mesozoic sandstones downgradient and parallel to the KST, flowpath length increases, and therefore, the potential to weather Mesozoic sandstones increases. Groundwater in the southern portion of the KST accumulates an elevated ⁸⁷Sr/⁸⁶Sr from Mesozoic sandstone as it flows from north to south. Groundwater that flows through Mesozoic sandstones mixes with CSM groundwater along the fault through fractures and areas of greater permeability.

Each of the five springs in the CSM flow region has a ⁸⁷Sr/⁸⁶Sr of 0.70831–0.70879 that falls within the range (0.70823–0.71200) and close to the median (0.70883) of geologic units present in the CSM. Comparison of spring ⁸⁷Sr/⁸⁶Sr to ⁸⁷Sr/⁸⁶Sr from rock leaching experiments indicates that Spring Mountains geology is the primary control on CSM geochemistry and that there is little to no flow from other Spring Mountains locations or regionally. Topography and published potentiometric contours (D'Agnese et al., 1998) also support this conclusion.

Similar to flow along the KST and the CSM, the elevation gradient and published potentiometric contours (D'Agnese et al., 1998) of the MH suggest that groundwater present along the Wheeler Pass Thrust flows from higher elevations at the northern extent of the thrust fault downgradient towards the southern extent of the thrust fault. Geochemical and isotopic comparisons of IES-005 and IES-064 support these proposed flowpaths. IES-005 groundwater is mixed between the CSM and MH flow groups. The spring emerges just northwest of the same thrust fault (Wheeler Pass Thrust Fault) that IES-064 (CSM flow group) emerges from but has a different geochemical signature and 87 Sr/ 86 Sr. IES-064 has a 87 Sr/ 86 Sr of 0.70864 and is a Ca-HCO $_3$ type water that predominately weathers limestones. In contrast, IES-005 has a ⁸⁷Sr/⁸⁶Sr of 0.71102 and is a Mg-HCO₃ type water that weathers both carbonate and silicate minerals. As groundwater flows south along the Wheeler Pass thrust it accumulates a silicate signature as the volume of up-gradient silicate rocks increases. The Bonanza King and Carrara Formations line the hanging wall of the thrust and facilitate mixing between the two flow groups. Comparison of IES-063 and IES-005 provides evidence for the importance of major pervasive thrust faults (i.e. KST & Wheeler Pass Thrust) in facilitating regional groundwater mixing. IES-007 and IES-008 are particularly distinct in ⁸⁷Sr/⁸⁶Sr. Both springs have very elevated ⁸⁷Sr/⁸⁶Sr (>0.73) than any of the rocks or springs in the study area. We hypothesize that groundwater flows through very radiogenic rocks prior to discharge in the spring and causes the unique chemistry of springs IES-007 and IES-008.

5.4. Conceptual model for three flow regions

5.4.1. Keystone Thrust groundwater

Groundwater discharging in the KST region is a combination of water recharged throughout the CSM and locally in the footwall region of the KST (Fig. 9). The evidence of a greater proportion of recharge by rain, extensive dedolomitization, and the mixed circulation depth signal of the Mg/Ca, along with the silicate weathering signature of ⁸⁷Sr/⁸⁶Sr indicate that KST groundwater undergoes significant flow through the Mesozoic sandstones in the footwall of the KST. The KST serves as a mixing zone between the CSM and footwall of the KST. Groundwater flows downgradient along the KST and accumulates an elevated ⁸⁷Sr/⁸⁶Sr from Mesozoic sandstones as it flows from north to south toward Death Valley.

5.4.2. Central Spring Mountains groundwater

Groundwater discharging in the CSM region is sourced by water recharged locally throughout the CSM. The evidence of a snow dominated recharge, extensive dedolomitization, and the shallow circulation depth signal of the Mg/Ca, along with ⁸⁷Sr/⁸⁶Sr that match local rocks indicate that CSM groundwater is recharged and discharges within the CSM. Published potentiometric contours (D'Agnese et al., 1998) decrease to the southwest, suggesting groundwater in the CSM flows downgradient toward Death Valley. Major thrust faults such as the Lee Canyon Thrust trend perpendicular to potentiometric contour lines and thus likely serve as conduits to flow because springs emerging at lower elevation on thrust faults undergo more dedolomitization and are high in total dissolved solids.

5.4.3. Montgomery Hills groundwater

Groundwater discharging in the MH region is a combination of snow recharged throughout the CSM and rain locally in the MH (Fig. 10). Groundwater in the MH exhibits a dedolomitization signature but also has ⁸⁷Sr/⁸⁶Sr similar to Cambrian and Pre-Cambrian siliciclastics (Fig. 5). This flow region is therefore likely weathering both siliciclastic rocks in the MH and limestone and dolostone present in the central

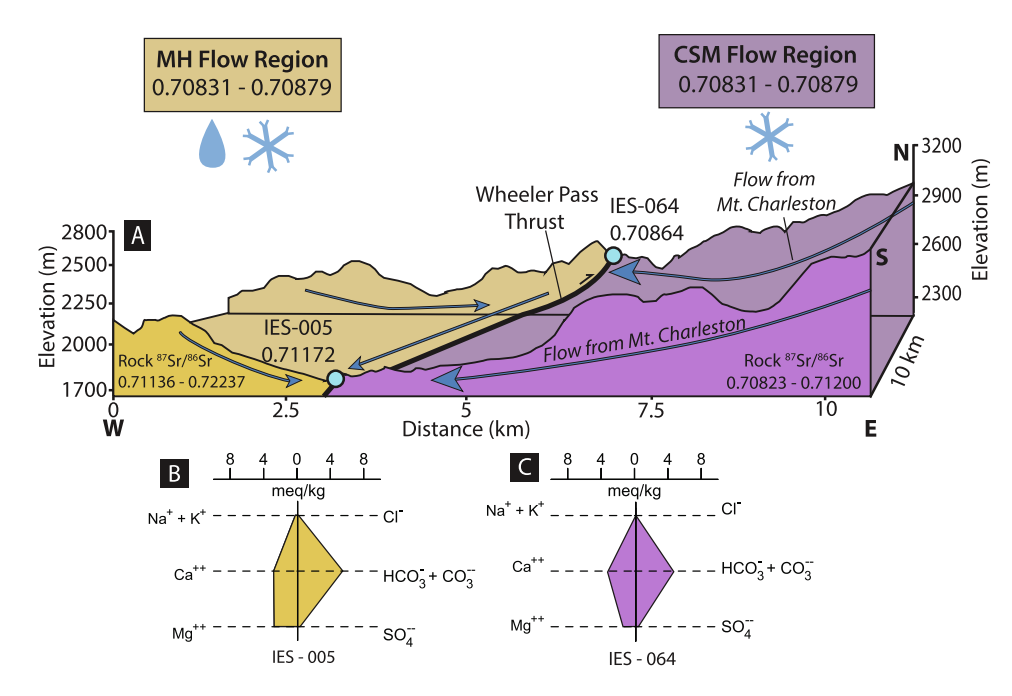


Fig. 10. A Simplified conceptual diagram of flowpaths contributing to springs along the Wheeler Pass Thrust with generalized locations of IES-005 and IES-064, arrow size approximates contribution of flow. Each flow region heading displays the range of $^{87}\mathrm{Sr}/^{86}\mathrm{Sr}$ for spring water in the region, dominant recharge mechanism is displayed below each heading. Yellow rocks are Cambrian and Precambrian siliciclastics, purple rocks are limestone and dolostone. Spring emergence locations are approximate, actual spring emergence elevations are lower. The northern section of the Wheeler Pass is higher in elevation than the southern Wheeler Pass Thrust. Groundwater emerging at IES-064 primarily weathers carbonate rocks as shown by the high concentrations of Ca²⁺, Mg²⁺, and HCO₃ in the stiff diagram, the $^{87}\mathrm{Sr}/^{86}\mathrm{Sr}$ of IES-064 is consistent with the carbonate and limestone to the east. Flow to IES-005 is sourced from two locations; 1) water flowing through dolostone and limestone that was recharged near Mt. Charleston, and 2) water flowing down-gradient along the Wheeler Pass Thrust after flow through the Montgomery Hills. Fig. 10B. Stiff diagram of IES-005.

Fig. 10C. Stiff diagram of IES-064. (For interpretation of the references to color in this figure legend, the reader is referred to the web version of this article.)

Spring Mountains. The Wheeler Pass Thrust fault divides the CSM and MH. IES-005 at the southwestern end of the fault exhibits a MH $^{87}\text{Sr}/^{86}\text{Sr}$ and Mg^{2+}/Ca^{2+} signature as well as a $\delta^{18}\text{O}$ and $\delta^{2}\text{H}$ from snow over the CSM, suggesting that the Wheeler Pass Thrust acts as a mixing zone between the two flow regions and that groundwater leaving the Spring Mountains is flowing down gradient toward Pahrump and Death Valley.

5.5. Implications for recharge to the Death Valley Regional Flow System

The Spring Mountains are identified as a recharge area for interbasin groundwater flow in the Death Valley region (Belcher et al., 2009; Belcher and Sweetkind, 2010; Bushman et al., 2010; Hevesi et al., 2003; Larsen et al., 2001; Stetzenbach et al., 1999; Thomas et al., 2013; Tiedeman et al., 2003; Winograd et al., 1998; Winograd and Pearson, 1976). Groundwater characteristics in the DVRFS were compared to observed Spring Mountains groundwater to both identify the area of recharge in the Spring Mountains most likely to contribute to the DVRFS and to predict the geochemistry and ⁸⁷Sr/⁸⁶Sr of groundwater leaving the Spring Mountains and flowing west towards Death Valley, the regional low.

The DVRFS contains twenty-five hydrogeologic units (Belcher and Sweetkind, 2010). The Spring Mountains hosts strata found in three of the hydrogeologic units: the sedimentary rock confining unit (SCU), the lower clastic-rock confining unit (LCCU), and the lower carbonate-rock aquifer (LCA). The SCU consists of cratonic sedimentary rocks with variable hydrogeologic properties and are observed in the footwall of the KST. Some of the SCU units may host groundwater flow, but these units are often disconnected or are too small or shallow to be significant contributors (Belcher and Sweetkind, 2010). The LCCU comprises Mesoproterozoic to Cambrian siliciclastic rocks and dolostone (Belcher and Sweetkind, 2010). The LCCU is a low hydraulic conductivity confining unit (Winograd and Thordarson, 1975). However, the LCCU has the potential for shallow groundwater contributions in places where it is highly fractured and brecciated (D'Agnese et al., 1998; Larsen et al., 2001). Fractured and brecciated quartzites were observed in the LCCU region of the northwest Spring Mountains while collecting rock samples for 87Sr/86Sr analysis, and these units are important to groundwater flow in the MH. The LCA is a thick aquifer containing Paleozoic carbonate units. The LCA contains the most permeable rocks in the DVRFS region; therefore, it is plausible that the LCA is a significant conduit groundwater flow. The LCA contains geologic units present throughout the Spring Mountains and it hosts the majority of strata in the CSM. Hydrogeologic characterizations such as large hydraulic conductivities (Belcher and Sweetkind, 2010; Winograd and Thordarson, 1975) suggest that the LCA has the highest potential to transport groundwater from the Spring Mountains to the Death Valley region with smaller flow components from the SCU and LCCU.

Many of the units present in the CSM are present in the regional LCA. These units include: Ely Spring Dolomite, Eureka Quartzite, Pogonip Group, Mississippian and Devonian rocks, Devonian rocks, Mountain Springs Formation, Nopah Formation, Bonanza King Formation, and the Carrara Formation (Belcher and Sweetkind, 2010). The units are primarily dolostone and limestone. Springs emerging in the Central Spring Mountains most closely match the expected weathering patterns of the carbonate units as illustrated in Fig. 5. The LCA has the largest spatial extent both at the surface and at depth in the CSM (as compared to the KST and MH). LCA units are present either at the surface or at depth across the entire CSM. In contrast, only the Carrara, Nopah, and Bonanza King formations are present in the MH. Similarly, the Nopah and Bonanza King formations outcrop across the entire KST.

Thrust faults serve as mixing zones between groundwater regions because two different rock types (silicates & dolostones) are next to one another in zones of fracturing. Pervasive dolostones at the thrust faults connect water from the silicate rocks to the DVRFS after mixing as indicated by groundwater emerging at thrust faults with 87Sr/86Sr signatures that reflect silicates in the KST or MH and $\delta^{18}O$ and $\delta^{2}H$ and geochemical signatures that reflect the CSM. The Bonanza King and Nopah Formations are present at the contacts between major thrust faults that divide the three flow groups (the KST and Wheeler Pass Thrust) and at the Lee Canyon Thrust in the CSM. The elevation of the thrust faults decreases to the southwest, implying that faults serve as conduits allowing groundwater to move to the southwest toward Death Valley. Some springs (IES-001, IES-002, IES-005) emerging along these thrust faults have ${}^{87}\mathrm{Sr}/{}^{86}\mathrm{Sr}$ indicative of silicate rocks despite emerging in or near thick regional dolostones. Geochemical observations from these springs flowing through the KST and MH suggest that these two silicate end members influence the geochemistry of groundwater in the Bonanza King and Nopah formations, and therefore, have the potential to influence the geochemistry of groundwater flowing toward Death Valley.

By combining observations of spring geochemistry and \$^8Sr/^86Sr with known hydrogeologic characteristics of the DVRFS, we developed a conceptual model that can predict groundwater flowpaths most likely to contribute to the DVRFS. Groundwater recharging in and around Mt. Charleston and flowing through the CSM contributes the greatest amount of flow to the DVRFS. Recharge along the KST or over the MH can reach the DVRFS after mixing at thrust faults; however, recharge from the KST and MH flow regions is less than the contribution from the CSM. We expect water leaving the Spring Mountains and flowing southwest to have a range from magnesium-bicarbonate waters to calcium-bicarbonate waters (Fig. 4).

6. Conclusion

Spring Mountains groundwater was grouped into three flow regions using 87 Sr/ 86 Sr, water δ^{18} O and δ^{2} H, and general geochemistry. Groundwater flow regions are distinguished as follows: 1) Keystone Thrust groundwater weathers both silicate and carbonate and has a ⁸⁷Sr/⁸⁶Sr of 0.710–0.711; 2) central Spring Mountains groundwater primarily weathers limestone and dolostone and has a 87Sr/86Sr of 0.708; 3) groundwater in the Montgomery Hills weathers both siliciclastics and carbonate and has ${}^{87}\mathrm{Sr}/{}^{86}\mathrm{Sr}$ 0.711–0.733. Groundwater flowing through the CSM has the highest potential to contribute to the DVRFS. Major thrust faults are conduits for groundwater flow and enable groundwater in the KST and MH flow regions to supplement flow from the Spring Mountains to the DVRFS. Mixing between groundwater regions occurs as groundwater flows downgradient, from northeast to southwest, along thrust faults. The relative contribution of groundwater from the three flow groups leaving the Spring Mountains could be more accurately quantified in future work by determining the $^{87}\mathrm{Sr}/^{86}\mathrm{Sr}$ and geochemistry of groundwater in deep wells throughout the Pahrump Valley and in the Tecopa basin and southern Death Valley that have not interacted with highly soluble basin fill.

Understanding groundwater in arid regions is important for ecosystems and communities that are dependent on groundwater resources for their primary freshwater supply, particularly as climate continues to change. The classification of recharge areas and groundwater flow direction presented in this paper are applicable to Spring Mountains ecosystems, the Las Vegas and Pahump water supplies, and the DVRFS. Methods used for identification of recharge source and dominant flowpaths have implications both locally and can be more broadly applied to groundwater flow in arid regions worldwide as groundwater in arid landscapes is often the only source of freshwater and subsequently it is difficult to directly observe and predict how freshwater resources are changing due to perturbations in climate and recharge patterns.

Author contributions

SRW designed the research plan, conducted field work to collect water samples, analyzed and interpreted the data, and wrote the paper. LKR secured funding and supervised the project, helped with the conceptualization of research goals and aims, assisted with hydrological field work and formal analysis of the data, and edited the manuscript and provided feedback on data presentation. ZPM provided assistance in the field and field work planning, helped with analysis and interpretation of data, and edited the manuscript. MDF secured funding for the project, assisted with hydrological field work and interpretation of the data, and edited the manuscript.

Declaration of Competing Interest

The authors declare that they have no known competing financial interests or personal relationships that could have appeared to influence the work reported in this paper.

Acknowledgements

Funding for this research was provided by the National Science Foundation (NSF) Grants 1516698 and 1516127. We thank the Humboldt-Toiyabe National Forest & Bureau of Land Management for permitting. We also thank Craig Lundstrom and UIUC for mass spectrometer use. We would like to thank IES members: Carolyn Gleason, Ariel Friel, Brian Hedlund, Khaled Pordel, and Katie Andrews for field assistance. We also thank Kurtis Burmeister for his helpful assistance. We thank two anonymous reviewers for their constructive comments and editor Huaming Guo for handling of the manuscript.

Funding

This work was supported by the National Science Foundation under grants 1516698 and 1516127.

Appendix A. Supplementary data

Supplementary data to this article can be found online at https://doi.org/10.1016/j.jhydrol.2019.124313.

References

- Akiyama, T., Kubota, J., Fujita, K., Tsujimura, M., Nakawo, M., Avtar, R., Kharrazi, A., 2018. Use of water balance and tracer-based approaches to monitor groundwater recharge in the hyper-arid Gobi Desert of northwestern China. Environments 5, 55. https://doi.org/10.3390/environments5050055.
- Al-Qudah, O.M., Woocay, A., Walton, J.C., 2017. Exploration of groundwater flowpaths and effective recharge in the Amargosa Desert, Nevada, using multivariate statistical analysis and elevation-dependent chloride mass-balance method. Environ. Earth Sci. 76, 110. https://doi.org/10.1007/s12665-017-6432-0.
- Anderson, K., Nelson, S., Mayo, A., Tingey, D., 2006. Interbasin flow revisited: the contribution of local recharge to high-discharge springs, Death Valley, CA. J. Hydrol. 323, 276–302. https://doi.org/10.1016/j.jhydrol.2005.09.004.
- Beitler, B., Parry, W.T., Chan, M.A., 2005. Fingerprints of Fluid flow: chemical diagenetic history of the Jurassic Navajo Sandstone, Southern Utah, U.S.A. J. Sediment. Res. 75, 547–561. https://doi.org/10.2110/jsr.2005.045.
- Belcher, W.R., Sweetkind, D.S., 2010. Death Valley Regional Groundwater Flow System, Nevada and California — Hydrogeologic Framework and Transient Groundwater Flow Model, Geological Survey Professional Paper 1711.
- Belcher, W.R., Bedinger, M.S., Back, J.T., Sweetkind, D.S., 2009. Interbasin flow in the Great Basin with special reference to the southern Funeral Mountains and the source of Furnace Creek springs, Death Valley, California, U.S. J. Hydrol. 369, 30–43. https://doi.org/10.1016/j.jhydrol.2009.02.048.
- Beria, H., Larsen, J.R., Ceperley, N.C., Michelon, A., Vennemann, T., Schaefli, B., 2018.
 Understanding snow hydrological processes through the lens of stable water isotopes.
 Wiley Interdiscip. Rev. Water 5, e1311. https://doi.org/10.1002/wat2.1311.
- Blum, J.D., Erel, Y., Brown, K., 1993. 87Sr/86Sr ratios of Sierra Nevada stream waters: implications for relative mineral weathering rates. Geochim. Cosmochim. Acta 57, 5019–5025. https://doi.org/10.1016/S0016-7037(05)80014-6.
- Blum, J.D., Gazis, C.A., Jacobson, A.D., Page Chamberlain, C., 1998. Carbonate versus silicate weathering in the Raikhot watershed within the High Himalayan Crystalline Series. Geology 26, 411. https://doi.org/10.1130/0091-7613(1998) 026 < 0411:CVSWIT > 2.3.CO;2.
- Bowen, G.J., Revenaugh, J., 2003. Interpolating the isotopic composition of modern meteoric precipitation. Water Resour. Res. 39, 1–13. https://doi.org/10.1029/
- Bowen, G.J., 2019. Gridded maps of the isotopic composition of meteoric waters. http://www.waterisotopes.org.
- Burbey, T.J., 1997. Hydrogeology and potential for ground-water development, carbonate-rock aquifers in southern Nevada and southeastern California, U.S. Geological Survey Water-Resources Investigations Report 95-4168.
- Burchfiel, B.C., Fleck, R.J., Secor, D.T., Vincelette, R.R., Davis, G.A., 1974. Geology of the Spring Mountains, Nevada. Bull. Geol. Soc. Am. 85, 1013–1022. https://doi.org/10. 1130/0016-7606(1974) 85 < 1013:GOTSMN > 2.0.CO;2.
- Bushman, M., Nelson, S.T., Tingey, D., Eggett, D., 2010. Regional groundwater flow in structurally-complex extended terranes: an evaluation of the sources of discharge at Ash Meadows, Nevada. J. Hydrol. 386, 118–129. https://doi.org/10.1016/j.jhydrol. 2010.03.013.
- Clow, D.W., Mast, M.A., Bullen, T.D., Turk, J.T., 1997. Strontium 87/strontium 86 as a tracer of mineral weathering reactions and calcium sources in an alpine/subalpine watershed, Loch Vale, Colorado. Water Resour. Res. 33, 1335–1351. https://doi.org/ 10.1029/97WR00856.
- D'Agnese, F.A., Faunt, C.C., Turner, A.K., 1998. An estimated potentiometric surface of the Death Valley region, Nevada and California, developed using geographic information system and automated interpolation techniques, U.S. Geological Survery Water-Resources Investigations Report 97-4052. p. 1–16.

Journal of Hydrology 580 (2020) 124313

Danapour, M., Højberg, A.L., Jensen, K.H., Stisen, S., 2019. Assessment of regional interbasin groundwater flow using both simple and highly parameterized optimization schemes. Hydrogeol. J. 1929–1947. https://doi.org/10.1007/s10040-019-01984-3.

S.R. Warix, et al.

- Dansgaard, W., 1964. Stable isotopes in precipitation. Tellus 16, 436–468. https://doi. org/10.1111/j.2153-3490.1964.tb00181.x.
- Dimmen, V., Rotevatn, A., Peacock, D.C.P., Nixon, C.W., Nærland, K., 2017. Quantifying structural controls on fluid flow: insights from carbonate-hosted fault damage zones on the Maltese Islands. J. Struct. Geol. 101, 43–57. https://doi.org/10.1016/j.jsg. 2017.05.012.
- Fossen, H., Zuluaga, L.F., Ballas, G., Soliva, R., Rotevatn, A., 2015. Contractional deformation of porous sandstone: insights from the Aztec Sandstone, SE Nevada, USA. J. Struct. Geol. 74, 172–184. https://doi.org/10.1016/j.jsg.2015.02.014.
- Frisbee, M.D., Tysor, E.H., Stewart-Maddox, N.S., Tsinnajinnie, L.M., Wilson, J.L., Granger, D.E., Newman, B.D., 2016. Is there a geomorphic expression of interbasin groundwater flow in watersheds? Interactions between interbasin groundwater flow, springs, streams, and geomorphology. Geophys. Res. Lett. 43, 1158–1165. https:// doi.org/10.1002/2015GI.067082.
- Frisbee, M.D., Meyers, Z.P., Stewart-Maddox, N.S., Caffee, M.W., Bogeholz, P., Hughes, M.N., 2017. What is the source of baseflow in agriculturally fragmented catchments? Complex groundwater/surface-water interactions in three tributary catchments of the Wabash River, Indiana, USA. Hydrol. Process. 31, 4019–4038. https://doi.org/10.1002/hyp.11345.
- Garrels, R.M., Mackenzie, F.T., 1967. Origin of the chemical compositions of some springs and lakes. In: Equilibrium Concepts in Natural Water Systems. American Chemical Society, Washington, DC, pp. 222–242. https://doi.org/10.1021/ba-1967-0067. ch010.
- Genereux, D., 1998. Quantifying uncertainty in tracer-based hydrograph separations. Water Resour. Res. 34, 915–919. https://doi.org/10.1029/98WR00010.
- Genereux, D.P., Wood, S.J., Pringle, C.M., 2002. Chemical tracing of interbasin ground-water transfer in the lowland rainforest of Costa Rica. J. Hydrol. 258, 163–178. https://doi.org/10.1016/S0022-1694(01)00568-6.
- Genereux, D.P., Nagy, L.A., Osburn, C.L., Oberbauer, S.F., 2013. A connection to deep groundwater alters ecosystem carbon fluxes and budgets: example from a Costa Rican rainforest. Geophys. Res. Lett. 40, 2066–2070. https://doi.org/10.1002/grl.50423.
- Harrill, J.R., 1986. Groundwater storage depletion in Pahrump Valley, Nevada-California, 1962-75, U.S. Geological Survey Water-Supply Paper 2279. DOI: 10.3133/ OFR81635.
- Hershey, R.L., 1989. Hydrogeology and Hydrogeochemistry of the Spring Mountains, Clark County, Nevada. Master's Thesis. University of Nevada, Las Vegas. Hershey, R.L., Fereday, W., Thomas, J.M., 2016. Dissolved organic carbon 14C in
- Hershey, R.L., Fereday, W., Thomas, J.M., 2016. Dissolved organic carbon 14C in southern Nevada groundwater and implications for groundwater travel times. Desert Res. Institute. Publ No 45268.
- Hevesi, B.J.A., Flint, A.L., Flint, L.E., 2003. Simulation of net infiltration and potential recharge using a distributed-parameter watershed model of the Death Valley region, Nevada and California, U.S. Geological Survey Water-Resources Investigations Report 03:4090.
- Hughes, J.L., 1966. Some aspects of the Hydrogeology of the Spring Mountains and Pahrump Valley, Nevada, and Environs, as determined by Spring Evaluation. Master's Thesis. Mackay School of Mines.
- Jacobson, A.D., Blum, J.D., Chamberlain, C.P., Poage, M.A., Sloan, V.F., 2002. Ca/Sr and Sr isotope systematics of a Himalayan glacial chronosequence: carbonate versus silicate weathering rates as a function of landscape surface age. Geochim. Cosmochim. Acta 66, 13–27. https://doi.org/10.1016/S0016-7037(01)00755-4.
- Johnson, T.M., Roback, R.C., McLing, T.L., Bullen, T.D., DePaolo, D.J., Doughty, C., Hunt, R.J., Smith, R.W., De Wayne, C.L., Murrell, M.T., 2000. Groundwater "fast paths" in the Snake River Plain aquifer: radiogenic isotope ratios as natural groundwater tracers. Geology 28, 871–874. https://doi.org/10.1130/0091-7613(2000) 28 < 871-GFPITS > 2,0.00-2.
- Klausmeyer, K., Howard, J., Keeler-wolf, T., Davis-fadtke, K., Hull, R., 2018. Mapping indicators of groundwater dependent ecosystems in California: Methods report. San Francisco, California.
- Kreamer, D.K., Stevens, L.E., Ledbetter, J.D., 2015. Groundwater dependent ecosystems science, challenges, and policy directions. Groundwater 205–230.
- Langman, J.B., Ellis, A.S., 2010. A multi-isotope (δD, δ18O,87Sr/86Sr, and δ11B) approach for identifying saltwater intrusion and resolving groundwater evolution along the Western Caprock Escarpment of the Southern High Plains, New Mexico. Appl. Geochem. 25, 159–174. https://doi.org/10.1016/j.apgeochem.2009.11.004.
- Larsen, D., Swihart, G.H., Xiao, Y., 2001. Hydrochemistry and isotope composition of springs in the Tecopa basin, southeastern California, USA. Chem. Geol. 179, 17–35. https://doi.org/10.1016/S0009-2541(01)00313-8.
- Las Vegas Valley Water District, 2018. Water Quality Report: Las Vegas Valley Water District.
- Liu, F., Williams, M.W., Caine, N., 2004. Source waters and flow paths in an alpine catchment, Colorado Front Range, United States. Water Resour. Res. 40, 1–16. https://doi.org/10.1029/2004WR003076.
- Love, A., Zdon, A., 2018. Use of radiocarbon ages to narrow groundwater recharge estimates in the Southeastern Mojave Desert, USA. Hydrology 5, 51. https://doi.org/10.3390/hydrology5030051.
- McKenna, O.P., Sala, O.E., 2018. Groundwater recharge in desert playas: current rates and future effects of climate change. Environ. Res. Lett. 13. https://doi.org/10.1088/ 1748-9326/aa9eb6.
- Meixner, T., Manning, A.H., Stonestrom, D.A., Allen, D.M., Ajami, H., Blasch, K.W., Brookfield, A.E., Castro, C.L., Clark, J.F., Gochis, D.J., Flint, A.L., Neff, K.L., Niraula, R., Rodell, M., Scanlon, B.R., Singha, K., Walvoord, M.A., 2016. Implications of projected climate change for groundwater recharge in the western United States. J. Hydrol. 534, 124–138. https://doi.org/10.1016/j.jhydrol.2015.12.027.

- Moreo, M.T., Senay, G.B., Flint, A.L., Damar, N.A., Laczniak, R.J., Hurja, J., 2014.Hydroclimate of the Spring Mountains and Sheep Range, Clark County, Nevada, U.S.Geological Survey Scientific Investigations Report 2014–5142.
- Morgan, D.S., Dettinger, M.D., 1994. Ground-water conditions in Las Vegas Valley, Clark County, Nevada; part II, Hydrogeology and simulation of ground-water flow. Open-File Rep. https://doi.org/10.3133/ofr90179.
- Négrel, P., Pauwels, H., Chabaux, F., 2018. Characterizing multiple water-rock interactions in the critical zone through Sr-isotope tracing of surface and groundwater. Appl. Geochem. 93, 102–112. https://doi.org/10.1016/j.apgeochem.2018.04.006.
- Nelson, S.T., Anderson, K., Mayo, A.L., 2004. Testing the interbasin flow hypothesis at Death Valley, California. Eos Trans. AGU 85 (37), 349–356 10.1029/2004E0370002. Eos (Washington. DC). doi: 10.1029/2005E0320005.
- Nelson, S.T., Mayo, A.L., 2014. The role of interbasin groundwater transfers in geologically complex terranes, demonstrated by the Great Basin in the western United States. Hydrogeol. J. 22, 807–828. https://doi.org/10.1007/s10040-014-1104-6.
- NOAA-NCDC, 2019. National Climate Data Center http://www.ncdc.noaa.gov/oa/ climate/onlineprod/ drought/xmgr.html.
- Nye County Water District, 2018. Pahrump Basin 162 Groundwater Management Plan. https://doi.org/http://www.nyecountywaterdistrict.net/DocumentCenter/View/118/Feb-2018-GWMP?bidId=.
- Paces, James B, Peterman, Zell E., Futa, Kiyoto, Oliver, Thomas A., Marshall, B.D., 2007. Strontium isotopic composition of Paleozoic carbonate rocks in the Nevada Test Site vicinity, Clark, Lincoln, and Nye Counties, Nevada, and Inyo County, California: U.S. Geological Survey Data Series 280.
- Pacheco, F.A.L., 2015. Regional groundwater flow in hard rocks. Sci. Total Environ. 506–507, 182–195. https://doi.org/10.1016/j.scitotenv.2014.11.008.
- Pacheco, F.A.L., Van der Weijden, C.H., 2014a. Modeling rock weathering in small watersheds. J. Hydrol. 513, 13–27. https://doi.org/10.1016/j.jhydrol.2014.03.036.
- Pacheco, F.A.L., Van der Weijden, C.H., 2014b. Role of hydraulic diffusivity in the decrease of weathering rates over time. J. Hydrol. 512, 87–106. https://doi.org/10.1016/j.jhydrol.2014.02.041.
- Page, W.R., Lundstrom, S.C., Harris, A.G., Langenheim, V.E., Workman, J.B., Mahan, S., Paces, J.B., Dixon, G.L., Rowley, P.D., Burchfiel, B.C., Bell, J.W., Smith, E.I., 2005. Geologic and geophysical maps of the Las Vegas 30' x 60' quadrangle Clark and Nye counties, Nevada, and Inyo County, California. Sci. Investig. Map. https://doi.org/10.3133/sim2814.
- Patten, D.T., Rouse, L., Stromberg, J.C., 2008. Isolated spring wetlands in the Great Basin and Mojave deserts, USA: potential response of vegetation to groundwater withdrawal. Environ. Manage. 41, 398–413. https://doi.org/10.1007/s00267-007-9035-9
- Penna, D., Engel, M., Mao, L., Dell'agnese, A., Bertoldi, G., Comiti, F., 2014. Tracer-based analysis of spatial and temporal variations of water sources in a glacierized catchment. Hydrol. Earth Syst. Sci. 18, 5271–5288. https://doi.org/10.5194/hess-18-5271-2014.
- Peterman, Z.E., Stuckless, J.S., Mahan, S.A., Marshall, B.D., Gutentag, E.D., Downey, J.S., 1992. Strontium isotope characterization of the Ash Meadows ground-water system, southern Nevada, USA. Low Temperature Environments In: 7th International Symposium on Water Rock Interaction Proceedings of the 7th International Symposium on Water-Rock Interaction, pp. 825–829.
- Pretti, V.A., Stewart, B.W., 2002. Solute sources and chemical weathering in the Owens Lake watershed, eastern California. Water Resour. Res. 38https://doi.org/10.1029/ 2001WR000370. 2-1-2-18.
- Pu, J., Yuan, D., Zhang, C., Zhao, H., 2012. Tracing the sources of strontium in karst groundwater in Chongqing, China: a combined hydrogeochemical approach and strontium isotope. Environ. Earth Sci. 67, 2371–2381. https://doi.org/10.1007/ s12665-012-1683-2.
- Rademacher, L.K., Clark, J.F., Hudson, G.B., Erman, D.C., Erman, N.A., 2001. Chemical evolution of shallow groundwater as recorded by springs, Sagehen basin; Nevada County, California. Chem. Geol. 179, 37–51. https://doi.org/10.1016/S0009-2541(01)00314-X.
- Raines, M.A., Dewers, T.A., 1997. Dedolomitization as a driving mechanism for karst generation in permian blaine formation, Southwestern Oklahoma, USA. Carbonates Evaporites 12, 24–31. https://doi.org/10.1007/BF03175799.
- Seymour, K.J., Ingram, J.A., Gebbett, S.J., 2008. Structural controls on groundwater flow in the Permo-Triassic sandstones of NW England. Geol. Soc. London Spec. Publ. 263, 169–185. https://doi.org/10.1144/gsl.sp.2006.263.01.09.
- Springer, A.E., Boldt, E.M., Junghans, K.M., 2016. Local vs. regional groundwater flow delineation from stable isotopes at western North America springs. Groundwater 55, 100–109. https://doi.org/10.1111/gwat.12442.
- Stetzenbach, K.J., Farnham, I.M., Hodge, V.F., Johannesson, K.H., 1999. Using multivariate statistical analysis of groundwater major cation and trace element concentrations to evaluate groundwater flow in a regional aquifer. Hydrol. Process. 13, 2655–2673. https://doi.org/10.1002/(SICI)1099-1085(19991215) 13:17 < 2655::AID-HYP840 > 3.0.CO;2-4.
- Stevenson, R., Pearce, C.R., Rosa, E., Hélie, J.-F., Hillaire-Marcel, C., 2018. Weathering processes, catchment geology and river management impacts on radiogenic (87Sr/86Sr) and stable (888/86Sr) strontium isotope compositions of Canadian boreal rivers. Chem. Geol. 486, 50–60. https://doi.org/10.1016/j.chemgeo.2018.03.039.
- Stewart-Maddox, N.S., Frisbee, M.D., Andronicos, C.L., Genereux, D.P., Meyers, Z.P., 2018. Identifying the regional extent and geochemical evolution of interbasin groundwater flow using geochemical inverse modeling and ⁸⁷Sr/⁸⁶Sr ratios in a complex conglomeratic aquifer. Chem. Geol. 500, 20–29. https://doi.org/10.1016/j.chemgeo.2018.07.026.
- Thomas, J.M., Moser, D.P., Fisher, J.C., Reihle, J., Wheatley, A., Hershey, R.L., Baldino, C., Weissenfluh, D., 2013. Using water chemistry, isotopes and microbiology to evaluate groundwater sources, flow paths and geochemical reactions in the Death

- $\label{lem:valley} Valley Flow System, USA. Procedia Earth Planet. Sci. 7, 842–845. \\ https://doi.org/10.1016/j.proeps.2013.03.033.$
- Tiedeman, C.R., Hill, M.C., D'Agnese, F.A., Faunt, C.C., 2003. Methods for using groundwater model predictions to guide hydrogeologic data collection, with application to the Death Valley regional groundwater flow system. Water Resour. Res. 39, 1–16. https://doi.org/10.1029/2001WR001255.
- Tóth, J., 1963. A theoretical analysis of groundwater flow in small drainage basins. J. Geophys. Res. 68, 4795–4812. https://doi.org/10.1029/jz068i016p04795.
- Tóth, J., 1995. Hydraulic continuity in large sedimentary basins. Hydrogeol. J. 3, 4–16. https://doi.org/10.1007/s100400050250.
- Tóth, J., 1999. Groundwater as a geologic agent: An overview of the causes, processes, and manifestations. Hydrogeol. J. 7, 1–14. https://doi.org/10.1007/s100400050176.
- Vittecoq, B., Reninger, P.A., Violette, S., Martelet, G., Dewandel, B., Audru, J.C., 2015. Heterogeneity of hydrodynamic properties and groundwater circulation of a coastal andesitic volcanic aquifer controlled by tectonic induced faults and rock fracturing – Martinique island (Lesser Antilles - FWI). J. Hydrol. 529, 1041–1059. https://doi. org/10.1016/j.jhydrol.2015.09.022.
- Winograd, I.J., Thordarson, W., 1975. Hydrogeologic and hydrochemical framework,

- south-central Great Basin, Nevada-California, with special reference to the Nevada Test Site, U.S. Geological Survey, Professional Paper.
- Winograd, I.J., Pearson, F.J., 1976. Major carbon 14 anomaly in a regional carbonate aquifer: possible evidence for megascale channeling, South Central Great Basin. Water Resour. Res. 12, 1125–1143. https://doi.org/10.1029/WR012i006p01125.
- Winograd, I.J., Riggs, A.C., Coplen, T.B., 1998. The relative contributions of summer and cool-season precipitation to groundwater recharge, Spring Mountains, Nevada, USA. Hydrogeol. J. 6, 77–93. https://doi.org/10.1007/s100400050135.
- Workman, J.B., Menges, C., Fridrich, C.J., Thompson, R.A., 2016. Geologic Map of Death Valley National Park, Nevada and California. In: Geological Society of America Annual Meeting, https://doi.org/10.1130/abs/2016AM-286651.
- Ye, M., Wang, L., Pohlmann, K.F., Chapman, J.B., 2016. Evaluating groundwater interbasin flow using multiple models and multiple types of data. Groundwater 54, 805–817. https://doi.org/10.1111/gwat.12422.
- Zieliński, M., Dopieralska, J., Belka, Z., Walczak, A., Siepak, M., Jakubowicz, M., 2017. The strontium isotope budget of the Warta River (Poland): between silicate and carbonate weathering, and anthropogenic pressure. Appl. Geochem. 81, 1–11. https://doi.org/10.1016/j.apgeochem.2017.03.014.